Bulletin of the New Zealand Society for Earthquake Engineering, Vol. 58, No. 3, September 2025

INVESTIGATING THE IMPACTS OF DESIGN DUCTILITY VALUES AND IMPORTANCE LEVELS ON THE PERFORMANCE OF BASE-ISOLATED BUILDINGS IN NEW ZEALAND

Claire Dong[1], Timothy J. Sullivan[2] and Didier Pettinga[3]

(Submitted *May 2024*; Reviewed *August 2024*; Accepted *October 2024*)

ABSTRACT

This study investigates the performance of base-isolated buildings designed according to the recommendations provided in the NZSEE/MBIE base isolation design guidelines. In total 16 case study buildings were designed for a site in Wellington, New Zealand, including four fixed-base buildings (for comparison) and 12 isolated buildings with various inelastic-spectrum-scaling factors, k_μ (equivalent to force-reduction factors) and importance levels. The performance of each building design was subsequently assessed using the FEMA P-58 framework. Three-dimensional numerical models were developed in OpenSees to perform the non-linear time history analysis with 180 pairs of ground motions across nine intensity levels. Results suggest that the average annual rate of collapse and the expected annual loss of the isolated buildings are both around four times lower than fixed-base buildings. This study also investigated the impacts of superstructure design ductility (controlled via the inelastic-spectrum-scaling factor, k_μ) and the design importance level. Results showed that a high k_μ is likely to worsen the performance of the base-isolated building. For a $k_\mu = 2$, the peak storey drift demands were increased by 50% ~ 100%, whereas the peak floor acceleration demands were only slightly reduced. As a result, the expected annual loss increased. Observations showed an increase in k_μ reduced the median value of the superstructure collapse fragility and could change the failure mechanism from isolator failure to superstructure failure. To improve performance, one could allow for more isolator displacement capacity at $k_\mu = 1$ or impose suitable superstructure deformation limits if a higher k_μ is permitted. Lastly, the results showed that designing a base-isolated building with a higher importance level increased the peak floor acceleration demands by 50% to 60% and had a mixed impact on the peak storey drift demands. However, it did reduce the annual rate of collapse rate by around a factor of two.

https://doi.org/10.5459/bnzsee.1693

INTRODUCTION

Base isolation can help enhance the performance of buildings in earthquakes [1]–[3]. A base-isolated building generally consists of a superstructure, isolation devices, connection elements above and below the isolators, foundation, and rattle space. The isolators are much more flexible compared to the superstructure; hence the majority of the dispalcement is expected to concentrate at the isolation layer. The flexible layer of isolators also results in an elongation in the system's fundamental period, which reduces the overall base shear demand. In addition, isolators such as friction pendulum devices, lead rubber bearings, or high damping rubber bearings are designed to dissipate seismic energy. Therefore, if designed properly, the isolation system can reduce the seismic demand transferred to the superstructure and hence achieve better seismic performance.

As base isolation is a widely used technique, its design process has been outlined in many design codes, such as the ASCE/SEI 7-22 [4] in the United States and Eurocode 8 [5] in Europe. Currently in New Zealand, base isolation is considered as an Alternative Solution design approach as it is not covered by the Acceptable Solutions and Verification Methods documented in the NZ building code [6]. In 2019, the New Zealand Society for Earthquake Engineering (NZSEE) released the "*Guideline for the Design of Seismic Isolation Systems for Buildings*" [7]. This guideline is a preliminary version for trial use and industry comments. Its ultimate goal is to provide more consistency in terms of the base isolation design process and performance outcomes across base-isolated buildings in New Zealand.

Previous international studies into the seismic performance of base-isolated buildings have given mixed results. Iervolino [8] found that base-isolated buildings in Italy have a relatively high global collapse rate compared to other new building typologies. However, other studies, including numerical studies in NZ by [9]–[11], as well as observations from past earthquakes [12]–[14], suggest that base-isolated buildings can perform well. Nevertheless, it is recognised that the performance of base-isolated buildings could be significantly affected by design decisions and the NZSEE base-isolation guidelines have not undergone thorough testing. As such, this study investigates some of the design choices and criteria that can affect isolated building design results and performance. These include building importance level and the New Zealand Standard (NZS) 1170.5:2004 [15] k_μ factor (design force-reduction factor). To achieve this, a set of case study buildings is designed in line with the NZ base isolation design guidelines and the likely performance of the buildings is subsequently assessed.

BASE-ISOLATED BUILDING DESIGN CONCEPTS

The NZSEE/MBIE guidelines [7] for base-isolated buildings effectively require consideration of a few key components, as illustrated in Figure 1; namely: foundation, rattle space,

[1] *Corresponding Author, PhD candidate, University of Canterbury, Christchurch, claire.dong@pg.canterbury.ac.nz (Member)*
[2] *Professor, University of Canterbury, Christchurch (Member)*
[3] *Technical Director, Holmes NZ LP, Christchurch*

isolation plane (including isolators and connection elements above and below the isolators), and the superstructure. The building design in this study is conducted only to the point of sizing the isolators and superstructure, as they are more likely to govern the design of other detailed elements and the system behaviour. In addition, it is assumed that the clearance around the isolated building is sufficient and therefore does not limit the design of the isolation plane. The rattle space is sized to accommodate the maximum displacement estimated using the guidelines [7].

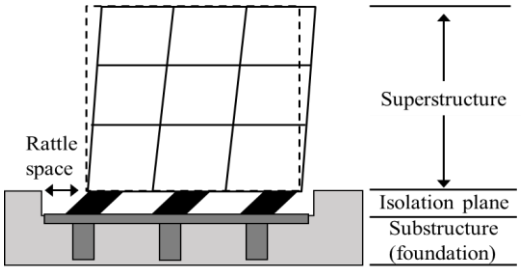

Figure 1: Key components within an isolated building.

Performance Objectives and Design Checks

The building performance objectives according to the New Zealand Building Code B1 [6] are to (a) safeguard people from injury caused by structural failure; (b) safeguard people from loss of amenity caused by structural behaviour; and (c) protect other property from physical damage caused by structural failure. To achieve these performance objectives, the NZS 1170.0:2002 [16] specifies limit states, as well as the loading and design checks at these limit states. The limit states include the Serviceability Limit State (SLS1/SLS2) and the Ultimate Limit State (ULS). The NZSEE/MBIE base isolation design guidelines [7] list two additional limit states, namely, a Damage Control Limit State (DCLS) and a Collapse Avoidance Limit State (CALS). At the DCLS, some damage is acceptable, but the cost of repair should be relatively low. The isolated building performance objective at DCLS appears to be subjective and will typically be agreed on by the engineers and clients. At the CALS, the intensity of the earthquake is also known as the Maximum Considered Earthquake (MCE). The isolated building should have a reasonable margin to limit the chances of collapse at the MCE load.

Based on the basic building information such as the dimensions, regularity, importance level, and design ductility, the building can be categorised according to the base-isolation guidelines into the following four types:

- Type 1: Simple, low-rise regular buildings that are designed for elastic actions ($k_\mu = 1$) and detailed for limited ductility.
- Type 2: General, building dimensions or height exceeds Type 1 but still regular, buildings can be designed for nominally ductile actions ($k_\mu \leq 1.25$) and detailed for limited ductility.
- Type 3: Complex or Ductile, building layout is complex or designed for ductile actions ($k_\mu \leq 2$), full capacity design and ductile detailing is expected. Importance level 4 buildings are also considered as Type 3 buildings.
- Type 4: Brittle, building has no ductility capacity.

As the building's complexity or design ductility increases, more comprehensive analysis methods should be used. For instance, it is sufficient to analyse a Type 1 building with the Equivalent Static Analysis (ESA) method, but Non-Linear Time History Analysis (NLTHA) is also required to verify the design of a Type 3 building.

Specific design checks are required to ensure the structure system has adequate strength, stiffness, and deformation capacity. The design checks for the isolation plane and superstructure are listed in Tables 1 and 2. According to the guidelines, unless specified, they should be evaluated considering the nominal, lower-bound, and upper-bound isolator properties.

Table 1: Isolation design checks for the case study buildings at various limit states.

Limit state	Design checks
ULS	- The effective period is less than 3s* (nominal) - The isolation system effective stiffness at ULS displacement is greater than 1/3 of the effective stiffness at 20% ULS displacement * (nominal) - Shear strain ≤ 200% - Factor of safety against Buckling ≥ 1.5
CALS	- Restoring force at 50% CALS displacement is 2.5% of the superstructure weight greater than the force at 100% CALS displacement (nominal) - 5% < effective damping < 30% (nominal) - Shear strain ≤ 250% - Overlapped area ≥ 25% - Factor of safety against Buckling ≥ 1.25 - Rattle space check

**Applied to Type 1 – Simple buildings*

Table 2: Superstructure design checks for the case study buildings at various limit states.

Limit state	Design checks
SLS1	- Superstructure responds elastically
DCLS	- Storey drift ≤ 0.5% **
ULS	- The effective isolation period is greater than 3 times the fixed superstructure period* (nominal) - Storey drift ≤ 2.5% (including P-delta effects) - Superstructure strength checks, e.g. plastic hinge flexural strength, member shear strength, axial strength, etc.

** Applied to Type 1 – Simple buildings, **Optional drift limit*

Design Seismic Demand

The guidelines adopt the method provided in NZS 1170.5:2004 [15] to estimate the seismic acceleration and displacement demand with a few modifications. The corner period at which the response spectrum changes to a constant-displacement is increased from 3s to up to 10s across various regions in New Zealand, to reflect the possible underestimation of the long-period spectral accelerations in NZS 1170.5:2004. The site hazard spectrum for horizontal loading (C(T)) is estimated using Equation (1).

$$C(T) = C_h(T) \cdot Z \cdot N(T, D) \cdot R \cdot \eta \qquad (1)$$

T is the effective period of the isolation system. $C_h(T)$ is the spectral shape factor which is a function of site subsoil class and effective period. Z is the hazard factor that indicates the seismicity of the location. N(T, D) is the near-fault factor that considers the effects if the location is close to the faults. η is the damping reduction factor which accounts for the energy dissipated by the isolators or damping devices. R is the return period factor that scales the spectra based on the return period of a given intensity (i.e. the inverse of the annual probability of exceedance). For example, R = 1 corresponds to an annual rate of exceedance of 1/500. The R factor depends on which limit

state is been analysed and the building importance level. Each building must be assigned an importance level ranging from 1 to 4 [16]. The importance level is related to the consequences of the structural failure and the required functionality post-disaster. For example, a 4-storey residential building may be classified as an IL2 building, and the design intensities for the SLS1 and ULS limit states correspond to return periods of 25 and 500 years, respectively. A 4-storey hospital may instead be classified as an IL4 building, the design intensities for the SLS2 and ULS limit states correspond to return periods of 500 and 2500 years, respectively. The design spectra are based on SA_{larger} which is the larger of the two as-recorded components [17]. While Equation (1) calculates the horizontal site hazard spectrum, Equation (2) defines the horizontal design spectrum ($C_d(T)$).

$$C_d(T) = \frac{C(T)S_p}{k_\mu} \quad (2)$$

Where S_p is the structural performance factor that, according to NZS 1170.5:2004 [15], is intended to account for a range of effects including higher material strength, strain hardening, structural redundancy, damping from non-structural elements, etc. For the isolation system and superstructure design, a S_p factor ranging from 0.7 to 1.0 is suggested by the guidelines [7], depending on the building complexity and design methods. k_μ is the inelastic-spectrum-scaling factor that is related to the structural design ductility using the equal displacement and equal energy rules. Note that k_μ only applies to the superstructure and that $1 \leq k_\mu \leq 2$ is permitted in the base isolation guidelines for the ULS checks, although this depends on the level of design and verification analysis being undertaken [7].

Analysis Procedure and Methods

The design starts with an assumed isolation system layout including the location, number and size of the isolators. The capacity-spectrum approach [18] is performed to check the displacement capacity, strength, and stability of the isolation system. In order to apply the capacity spectrum approach, the capacity curve is computed assuming the superstructure responds as a rigid block, and the isolation system behaves as a Single Degree of Freedom (SDOF) system. A demand displacement is assumed at first to estimate the area-based effective damping. The damped Acceleration-Displacement Response Spectra (ADRS) can then be plotted together with the capacity curve. The intersection is the design acceleration and displacement demand on the isolation system. This process is iterated until the assumed displacement matches the design displacement at the intersection of the capacity and demand curves. The design base shear is then applied as a set of equivalent lateral forces on the superstructure. The strength and stiffness of the superstructure's lateral load resisting system, with allowance for ductile response according to the equivalent static method of NZS 1170.5:2004 [15] is then checked. Four load distribution patterns are recommended by the guidelines and the worst load case shall be used for design, including triangular, rectangular, a profile specified in NZS 1170.5:2004 [15], and a load pattern from ASCE/SEI 7-16 [19]. This design process is again iterated until all the checks listed in Tables 1 and 2 are satisfied.

CASE STUDY BUILDINGS DESIGN RESULTS

The case study buildings designed and assessed in this study are assumed to be in Wellington, New Zealand, with a V_{S30} of 450 m/s, which can be classified as subsoil class C according to NZS 1170.5:2004 [15]. All superstructures have the same footprint which is 24 m by 40 m. There are four storeys in each building, the first storey is 4.5 m, and the rest are 3.6 m, with a total height of 15.3 m. The building's seismic weight is estimated based on the preliminary design and may be refined later. The seismic weight is 14000 kN for the ground floor, 5303 kN for levels two to four, and 4658 kN for the roof, resulting in a total of 34566 kN. The breakdown of seismic weights can be found in [20].

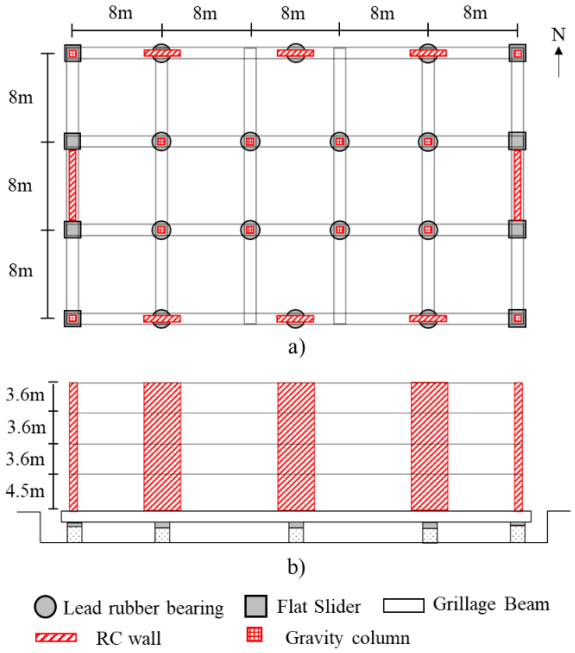

Figure 2: Structural layout of the reinforced concrete wall structure, a) plan view and b) south elevation.

Two superstructure typologies are investigated: Reinforced Concrete (RC) walls and steel Moment Resisting Frames (MRF). The lateral systems of the isolated RC wall buildings consist of six short walls in the EW direction and two longer walls in the NS direction, see Figure 2. The lateral systems of the isolated steel MRF buildings consist of four identical frames, two in each direction, see Figure 3. The type of connection used in the MRF design is the Reduced Beam Section (RBS). It is assumed that the gravity system will not provide lateral resistance and therefore is not designed in this study. The gravity columns are included in the models for the purpose of distributing the mass evenly and applying gravity loads for P-delta actions in later analysis. The isolation plane layouts for the RC wall structures and steel MRF structures are shown in Figures 2a and 3a, respectively. The base arrangements are chosen such that the FSs are located around the perimeter where significant compressive and uplifting forces are expected. In the interests of comparing building performance, the isolation system properties of the RC walls and steel MRF are kept similar, i.e. they are all isolated by 14 Lead Rubber Bearings (LRB) and 8 Flat Sliders (FS). The isolators are connected by grillage beams with a floor slab on top. Whilst detailed design of the grillage beams is not completed, they are sized to have sufficient stiffness so that their flexibility contributed only around 10%-15% of the roof displacement at yield, and to resist the moment demands from the superstructure. The flexibility of the grillage beams is included in both the design and assessment phases of this research. The structural layouts for each building typologies remain the same and the difference due to design parameters is reflected through member and isolator sizes. In addition, the buildings are also designed using conventional methods without base isolation. The conventional buildings are designed to meet the minimum building code requirement according to NZS 1170.5:2004 [15].

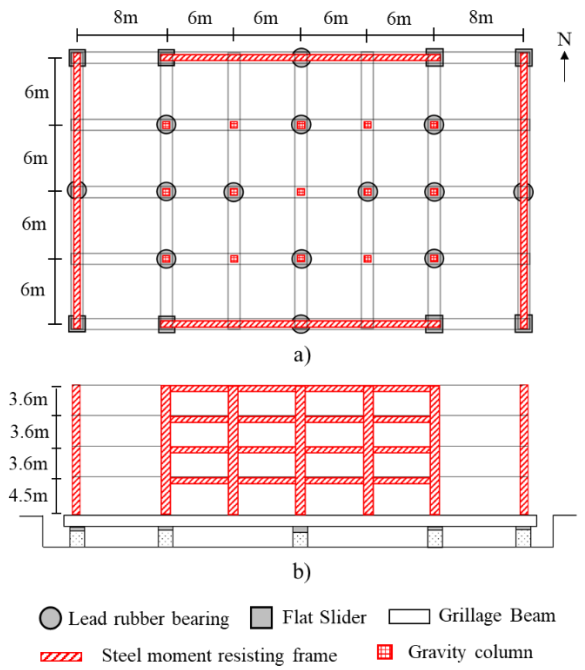

Figure 3: Structural layout of the steel moment resisting frame structure, a) plan view and b) south elevation.

Design Results

The design results obtained for the case study buildings are presented in this section. As mentioned previously, the isolated buildings can be categorised into four types according to the guidelines [7]. The IL2 case study buildings (with $k_\mu = 1$) are classified as Type 1, and the minimum structural performance factor for the isolation system and superstructure are 1. Whereas the IL2 buildings (with $k_\mu = 2$) and IL4 buildings are classified as Type 3, meaning the minimum structural performance factor can be as low as 0.7. In this study, a structural performance factor of 1 is adopted for both isolation system ($S_{p,iso} = 1$) and superstructure ($S_{p,super} = 1$) for the isolated buildings designs. A $S_{p,super}$ factor of 0.7 is adopted for the traditional fixed-base ductile building designs as suggested by NZS 1170.5:2004 [15].

Table 3: Seismic design parameters that are used to construct the hazard spectrum for a site in Wellington according to NZS 1170.5:2004.

Seismic design parameters	IL2	IL4
Hazard factor, Z	0.4	0.4
Return period factor, R_{SLS1}	0.25	0.25
R_{DCLS}	0.75	1
R_{ULS}	1	1.8
R_{CALS}	1.5	2.34
Spectral shape factor, $C_h(T)$ *	0.56g	0.61g
Near-fault factor, N(T, D) *	1.21	1.16
Equivalent viscous damping, ξ *	27%	25%
Design base shear, $C_d(T)$ *	0.13g	0.26g

** Based on the ULS effective period assuming nominal isolator properties*

Since all of the buildings are designed for the same site, the hazard factor is identical. The difference in the seismic demand mostly comes from the return period factor, reflecting the different building importance levels. The seismic design parameters for the design spectrum are reported in Table 3. Some of these parameters depend on the effective period of the system and require the design to be iterative.

The capacity-spectrum analysis method is performed by plotting the capacity curve of the isolation system (as a SDOF system) against the ADRS for four limit states, see Figure 4. The isolation system design results are reported in Table 4 and the upper-bound and lower-bound isolator property modification factors are shown in Table 5. The concurrency of seismic actions and torsional effects have been accounted for when estimating the maximum displacement demands.

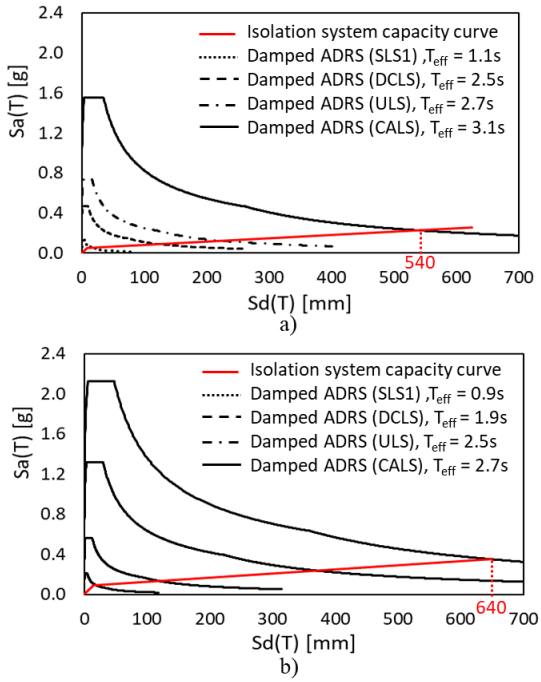

Figure 4: The capacity curves of the isolation systems based on lower-bound isolator properties and the acceleration-displacement response spectra for: a) IL2 and b) IL4.

Table 4: Case study building isolation system design results based on nominal isolator properties.

Isolation System Properties	IL2	IL4
No. of Lead rubber bearings	14	14
Lead rubber bearing dia. [mm]	900	1000
Lead core dia. [mm]	130	190
Total rubber thickness, t_e [mm]	252	252
No. of flat friction sliders	8	8
Friction coefficient at ULS	4%	4%
Characteristic strength, Q_d [kN]	2037	3764
Post-yield stiffness, K_d [kN/mm]	13.7	17.4
Stiffness ratio, α [K_d / K_i]	0.0577	0.0765

Table 5: Isolator property modification factors.

Variable		λ_{min}	λ_{max}
Ageing and environmental factors	LRB Q_d	1.00	1.00
	LRB K_d	1.00	1.10
	FS μ	1.00	1.21
Testing factors	LRB Q_d	0.95	1.30
	LRB K_d	0.98	1.03
	FS μ	0.95	1.15
Manufacturing variation	LRB Q_d	0.85	1.15
	LRB K_d	0.85	1.15
	FS μ	0.85	1.15
Total property multiplier	**LRB Q_d**	**0.81**	**1.50**
	LRB K_d	**0.83**	**1.27**
	FS μ	**0.81**	**1.60**

Table 6: Case study building superstructure design results for IL2 steel MRF structures.

Design scenario	Fixed-base	Base-isolated	Base-isolated	Base-isolated (DC)**
Importance level, IL	IL2	IL2	IL2	IL2
Performance factor, $S_{p,super}$	0.7	1	1	1
Column member sizes (Grade 300)				
Storey 4	310UC137	500WC228	350WC197	400WC270
Storey 3	310UC137	500WC228	350WC197	400WC270
Storey 2	310WC197	500WC340	350WC258	500WC228
Storey 1	310WC197	500WC340	350WC258	500WC228
Beam member sizes (Grade 300)				
Storey 4	410UB59.7	600UB101	530UB82	530UB92.4
Storey 3	460UB82.1	600UB113	600UB101	600UB113
Storey 2	530UB92.4	700WB150	700WB115	700WB130
Storey 1	530UB92.4	700WB150	700WB115	700WB130
Fixed-base period, $T_{fixed,x}$	1.49s	0.84s	1.17s	0.90s
First yield drift	0.75%	0.42%	0.54%	0.57%
SLS design base shear	1296 kN ($k_\mu = 1$)	3102 kN ($k_\mu = 1$)	3102 kN ($k_\mu = 1$)	3102 kN ($k_\mu = 1$)
ULS design base shear	1296 kN ($k_\mu = 4$)	4669 kN ($k_\mu = 1$)	1952 kN ($k_\mu = 2$)	1952 kN ($k_\mu = 2$)
ULS maximum storey drift	2.43 %	0.64%	1.34%	0.65%
Design governed by	ULS drift (2.5%)	$T_{eff} \geq 3 \times T_{fixed}$	SLS1 no yielding	DCLS drift (0.5%)

*** An additional drift limit (0.5%) is imposed at the DCLS*

Table 7: Case study building superstructure design results for IL4 steel MRF structures.

Design scenario	Fixed-base	Base-isolated	Base-isolated	Base-isolated (DC)**
Importance level, IL	IL4	IL4	IL4	IL4
Performance factor, $S_{p,super}$	0.7	1	1	1
Column member sizes (Grade 300)				
Storey 4	400WC181	500WC414	500WC290	500WC340
Storey 3	400WC181	500WC414	500WC290	500WC340
Storey 2	400WC270	500WC440	500WC383	500WC440
Storey 1	400WC270	500WC440	500WC383	500WC440
Beam member sizes (Grade 300)				
Storey 4	460UB82.1	800WB122	700WB115	700WB115
Storey 3	600UB101	800WB168	700WB130	800WB122
Storey 2	700WB115	900WB218	700WB150	800WB146
Storey 1	700WB130	900WB218	700WB173	800WB168
Fixed-base period, $T_{fixed,x}$	1.04s	0.67s	0.80s	0.74s
First yield drift	0.64%	0.52%	0.44%	0.46%
SLS design base shear	1662 kN ($k_\mu = 1$)	5141 kN ($k_\mu = 1$)	5141 kN ($k_\mu = 1$)	3102 kN ($k_\mu = 1$)
ULS design base shear	2992 kN ($k_\mu = 4$)	7575 kN ($k_\mu = 1$)	3788 kN ($k_\mu = 2$)	1952 kN ($k_\mu = 2$)
ULS maximum storey drift	2.40%	0.67%	1.34%	0.75%
Design governed by	ULS drift (2.5%)	ULS moment	SLS1 no yielding	DCLS drift (0.5%)

*** An additional drift limit (0.5%) is imposed at the DCLS*

Once the isolation system is designed, the design base shear estimated at the SLS, ULS, and DCLS (optional) are distributed to the superstructure using the ESA method. The NLTHA method is also applied to the Type 3 (complex and ductile) buildings to verify the building designs based on the ESA method, which are shown to be valid. The steel MRF member sizes, design parameters, and results are shown in Tables 6 and 7. Similarly, the RC wall dimensions, design parameters, and results are shown in Tables 8 and 9. For the RC walls, cracked stiffnesses [21] are applied when estimating the building period and drift demands. All periods are obtained using modal analysis. In addition, the design criteria that govern the RC wall dimensions, reinforcement, and steel MRF member sizes are also reported. Capacity design provisions are applied in all superstructure designs, using dynamic magnification factors and overstrength factors from NZ material standards [22], [23]. Gravity and wind loads have also been checked and were found to not govern the design and are thus, not discussed further here.

Based on the design results, a higher importance level leads to a higher design seismic demand in the isolation system, and therefore requires larger isolators with a higher characteristic strength, post-yield stiffness, and displacement capacity. This increases the effective stiffness of the isolation system at the design intensity level and results in a higher design base shear in the superstructure. Subsequently, the superstructure needs to be stronger and stiffer. However, when an inelastic-spectrum-scaling factor greater than one is applied, the required strength of the superstructure is reduced by allowing the superstructure to respond inelastically. There are a number of design scenarios that are governed by the SLS1 no yielding criterion. For fixed-base RC walls, the combination of k_μ and R factors would result in similar base shear demands at the SLS1 and ULS, except that according to NZS 3101.1&2:2006 [22], the wall stiffness at

SLS1 is higher than that at ULS, which resulted in a larger base shear. For isolated buildings, the superstructure base shear demands associated with SLS1 and ULS are not drastically different due to the low post-yield stiffness of the isolation system. Therefore, when applying a $k_{\mu,ULS} = 2$, the SLS1 base shear becomes more critical.

Table 8: Case study superstructure design results for IL2 RC wall structures.

Design scenario	**Fixed-base**	**Base-isolated**	**Base-isolated**	**Base-isolated (DC)****
Importance level, IL	IL2	IL2	IL2	IL2
Performance factor, $S_{p,super}$	0.7	1	1	1
		Longitudinal direction (E-W)		
Wall dimensions (per wall)	3.0 × 0.3 m	3.0 × 0.6 m	3.0 × 0.3 m	3.0 × 0.5 m
Nominal flexural strength, $M_{n,x}$	6712 kNm	15923 kNm	7423 kNm	13252 kNm
Long. reinforcement ratio, $\rho_{b,x}$	0.91%	1.31%	1.19%	1.31%
Axial load ratio	2.0%	1.5%	2.0%	1.6%
Fixed-base period, $T_{fixed,x}$	0.56s (1.19s) *	0.38s (0.80s) *	0.56s (1.18s) *	0.44s (0.88s) *
First yield drift	0.84%	0.82%	0.82%	0.81%
SLS design base shear	2465 kN ($k_\mu = 1$)	3102 kN ($k_\mu = 1$)	3102 kN ($k_\mu = 1$)	3102 kN ($k_\mu = 1$)
ULS design base shear	1431 kN ($k_\mu = 4$)	4669 kN ($k_\mu = 1$)	1952 kN ($k_\mu = 2$)	1952 kN ($k_\mu = 2$)
ULS maximum storey drift	1.99%	0.73%	1.38%	0.74%
Design governed by	SLS1 no yielding	$T_{eff} \geq 3 \times T_{fixed}$	SLS1 no yielding	DCLS drift (0.5%)
		Transverse direction (N-S)		
Wall dimensions (per wall)	6.0 × 0.3 m	6.0 × 0.3 m	6.0 × 0.3 m	6.0 × 0.3 m
Nominal flexural strength, $M_{n,y}$	29786 kNm	32066 kNm	25401 kNm	25401 kNm
Long. reinforcement ratio, $\rho_{b,y}$	1.19%	1.3%	0.94%	0.94%
Axial load ratio	1.9%	1.9%	1.9%	1.9%
Fixed-base period, $T_{fixed,y}$	0.36s (0.68s) *	0.34s (0.76s) *	0.36s (0.85s) *	0.36s (0.84s) *
First yield drift	0.43%	0.43%	0.43%	0.43%
SLS design base shear	3684 kN ($k_\mu = 1$)	3102 kN ($k_\mu = 1$)	3102 kN ($k_\mu = 1$)	3102 kN ($k_\mu = 1$)
ULS design base shear	2157 kN ($k_\mu = 4$)	4669 kN ($k_\mu = 1$)	1952 kN ($k_\mu = 2$)	1952 kN ($k_\mu = 2$)
ULS maximum storey drift	0.41%	0.57%	0.62%	0.60%
Design governed by	SLS1 no yielding	ULS moment	SLS1 no yielding	SLS1 no yielding

** The reported periods are based on the gross section stiffness and cracked section stiffness (in brackets), the cracked section stiffness is estimated according to* [21]. *** An additional drift limit (0.5%) is imposed at the DCLS*

Table 9: Case study building superstructure design results for IL4 RC wall structures.

Design scenario	Fixed-base	Base-isolated	Base-isolated	Base-isolated (DC)**
Importance level, IL	IL4	IL4	IL4	IL4
Performance factor, $S_{p,super}$	0.7	1	1	1
		Longitudinal direction (E-W)		
Wall dimensions (per wall)	3.0 × 0.5 m	3.0 × 0.6 m	3.0 × 0.4 m	3.0 × 0.6 m
Nominal flexural strength, $M_{n,x}$	11517 kNm	20142 kNm	12665 kNm	20142 kNm
Long. reinforcement ratio, $\rho_{b,x}$	1.05%	1.79%	1.64%	1.79%
Axial load ratio	1.6%	1.5%	1.7%	1.5%
Fixed-base period, $T_{fixed,x}$	0.44s (0.95s) *	0.38s (0.71s) *	0.49s (0.90s) *	0.39s (0.71s) *
First yield drift	0.81%	0.86%	0.84%	0.86%
SLS design base shear	3196 kN ($k_\mu = 1$)	5614 kN ($k_\mu = 1$)	5614 kN ($k_\mu = 1$)	5614 kN ($k_\mu = 1$)
ULS design base shear	3048 kN ($k_\mu = 4$)	7215 kN ($k_\mu = 1$)	4120 kN ($k_\mu = 2$)	4120 kN ($k_\mu = 2$)
ULS maximum storey drift	2.48%	0.85%	1.49%	0.93%
Design governed by	ULS drift (2.5%)	ULS moment	SLS1 no yielding	DCLS drift (0.5%)
		Transverse direction (N-S)		
Wall dimensions (per wall)	6.0 × 0.3 m	6 × 0.4 m	6 × 0.3 m	6 × 0.3 m
Nominal flexural strength, $M_{n,y}$	38209 kNm	59140 kNm	47723 kNm	47723 kNm
Long. reinforcement ratio, $\rho_{b,y}$	1.64%	2.01%	2.18%	2.18%
Axial load ratio	1.9%	1.7%	1.9%	1.9%
Fixed-base period, $T_{fixed,y}$	0.36s (0.63s) *	0.31s (0.62s) *	0.36s (0.68s) *	0.35s (0.67s) *
First yield drift	0.42%	0.45%	0.44%	0.42%
SLS design base shear	3684 kN ($k_\mu = 1$)	5614 kN ($k_\mu = 1$)	5614 kN ($k_\mu = 1$)	5614 kN ($k_\mu = 1$)
ULS design base shear	4488 kN ($k_\mu = 4$)	7215 kN ($k_\mu = 1$)	4120 kN ($k_\mu = 2$)	4120 kN ($k_\mu = 2$)
ULS maximum storey drift	1.84%	0.45%	0.068%	0.66%
Design governed by	ULS moment	ULS moment	SLS1 no yielding	SLS1 no yielding

** The reported periods are based on the gross section stiffness and cracked section stiffness (in brackets), the cracked section stiffness is estimated according to* [21]. *** An additional drift limit (0.5%) is imposed at the DCLS*

PERFORMANCE ASSESSMENT METHODOLOGY

With the building designs complete, the likely performance of the different case study design solutions is assessed in line with FEMA P-58 [24] (previously the Performance-Based Earthquake Engineering (PBEE) framework developed by the Pacific Earthquake Engineering Research (PEER) Centre [25]). The performance assessment requires inputs of structural response parameters such as Peak Floor Acceleration (PFA) and Peak Storey Drift (PSD); collapse fragility, annual rate of collapse and loss functions. The expected annual loss (EAL) can then be quantified via the FEMA P-58 procedure. Four stages of analyses were carried out in this study, including:

1. Hazard analysis; the hazard curve is determined and ground motions are selected accordingly.
2. Structural analysis; numerical models are constructed to perform the NLTHA, the structural responses such as PSD, PFA, hinge plastic rotation, and isolator displacement demands at intensity levels are recorded.
3. Damage analysis; damageable components and their fragility functions are identified, and the level of component or global damage is assessed using results from stage two.
4. Loss analysis; consequence functions (such as repair costs) are assigned to the damageable components. The loss is then estimated for each intensity level using the results from stage three.

Detailed descriptions and examples of the implementation of the PBEE PEER framework can be found in the literature [26]. The assessment procedure and examples are illustrated in this section.

Hazard Analysis and Ground Motion Selection

In the hazard analysis, hazard curves are determined and will inform the ground motion selection for NLTHA. In this work, the hazard curves for ground motion selection are based on the 2010 New Zealand National Seismic Hazard Model (NSHM) [27]. Spectral acceleration (Sa) corresponding to periods of 1s and 2s were selected as the conditioning intensity measure for the fixed-base and base-isolated buildings, respectively. The seismic hazard curves are shown in Figure 5. The ground motions were selected in a previous study [20], who used the generalised conditioning intensity measure approach [28] to ensure the ground motions are probabilistically consistent with the seismic hazard. The suite consists of 180 pairs of ground motions across nine intensity levels (20 pairs each). The intensity measure and annual rate of exceedance are reported in Table 10.

The case study buildings were designed based on the design hazard curves provided in NZS 1170.5:2004 [15], also plotted in Figure 5. The comparison suggests that for this specific site in Wellington, the design hazard curves overestimate the rates of small to moderate intensity earthquakes and underestimate the rates of moderate to large earthquakes. This highlights the importance of updating the design standard to incorporate the most recent hazard information. The latest revision of the NSHM was released in 2022 [29]. In the future, when the design standard is updated, the case study building design and ground motions may be updated. With that being said, the results from this study still provide valuable insight into the impacts of the inelastic-spectrum-scaling factor (design ductility) and design importance level on base-isolated building performance.

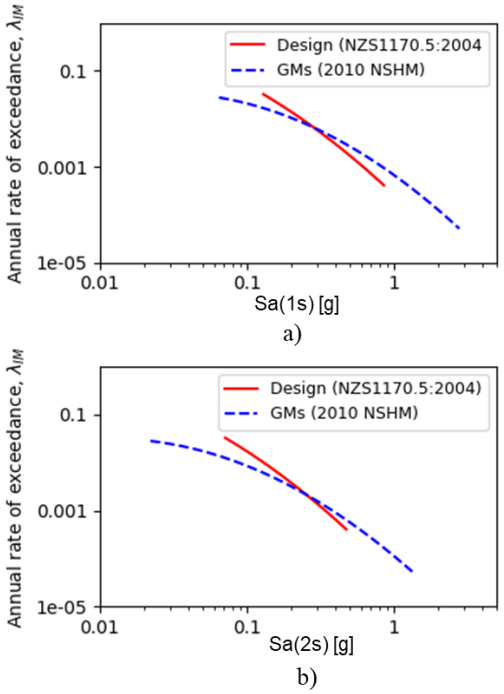

Figure 5: Design hazard curves and ground motion hazard curves for the Wellington site, a) spectral acceleration at 1.0s and b) spectral acceleration at 2.0s.

Numerical Models

The 3D numerical models of the case study buildings are built in OpenSees [30]. Probable material properties are assigned to reflect the expected characteristics. The RC superstructure model consists of walls and gravity frames, which are tied together by the floor diaphragms, as illustrated in Figure 6. The RC walls are modelled with the elastic Timoshenko beam elements [31] with an effective cracked section stiffness [21]. Rotational plastic hinges with Takeda hysteretic properties [32], shown in Figure 7, are placed at the bottom of the walls. No strength degradation is modelled for the walls. The initial and post-yield stiffnesses of the wall and hinge elements are calibrated to account for the "springs in series" effects. The gravity columns are modelled as elastic truss elements with reasonably large axial stiffness, to provide gravity support and allow application of gravity loads for P-Delta actions. No beams are modelled in the upper levels of the RC wall building, assuming that there is no coupling effect and walls act as cantilevers. The floor diaphragms are assumed to be rigid in-plane and constraint the vertical elements in the horizontal directions. The seismic mass and gravity load are applied at the RC wall and gravity frame nodes based on their tributary area.

Table 10: Ground motion information at each intensity.

	IL1	IL2	IL3	IL4	IL5	IL6	IL7	IL8	IL9
Annual exceedance rate, λ_{IM}	0.10000	0.03219	0.01386	0.00446	0.00211	0.00103	0.00040	0.00020	0.00010
Return period, RP [yrs]	31	72	224	475	975	2475	4975	9975	24975
SA (1s)	0.07g	0.13g	0.32g	0.57g	0.89g	1.36g	1.75g	2.17g	2.78g
SA (2s)	0.02g	0.05g	0.14g	0.26g	0.41g	0.63g	0.83g	1.04g	1.36g

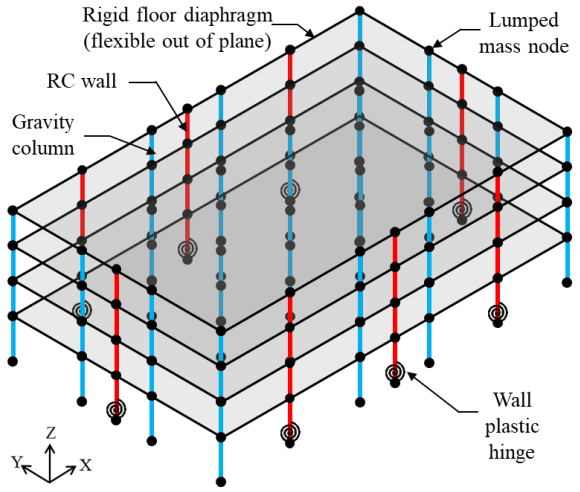

Figure 6: Idealisation of the numerical model of the reinforced concrete wall superstrcuture.

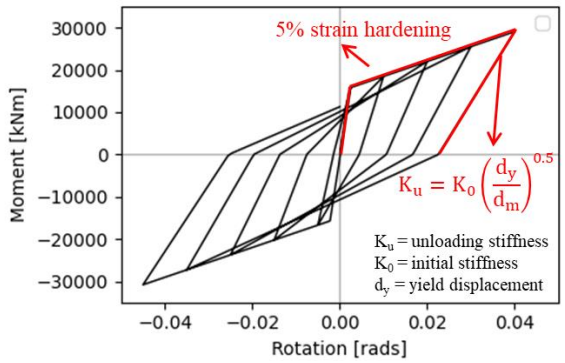

Figure 7: An example of RC wall plastic hinging modelled with the Takeda hysterestic model.

Rayleigh damping model is adopted in the numerical models. A 5% viscous damping is assigned to the first and the third modes. The damping is proportional to the last committed tangent stiffness. Note that the Rayleigh damping is only applied to the superstructure to represent the superstructure energy dissipation. The energy dissipation in the isolation devices is accounted for separately and does not contribute to the Rayleigh damping to avoid the damping leakage phenomenon [33]. While there is uncertainty as to the best means of modelling damping [34]–[36], it is considered that the choice of damping model will not affect the relative performance assessment being conducted here.

The steel MRF superstructure model shown in Figure 8 consists of four identical moment resisting frames, gravity columns, and beams that are again tied together by floor diaphragms that are assumed to behave rigidly in-plane. The connection details of the beams, columns, and joints are presented in Figure 9. The beam and column members are modelled as elastic Timoshenko beam elements [31]. The beam hinges are located a certain distance away from the column faces to reflect the behaviour of RBS moment connections, whereas the potential column hinges are located at the beam faces. A rotational spring is placed at the centre of the beam-column joint to capture joint zone deformation.

The modified Ibarra-Median-Krawinkler deterioration model is used to model the beam and column hinges [37]. For RBS hinges, the moment-rotation curves, including the cyclic deterioration parameters are estimated based on the equations proposed by [38]. Whereas the moment-rotation curves for column hinges are estimated based on [39]. An example of such a beam and column hinge is shown in Figure 10. Note that for the sake of numerical convergence and computational efficiency, a large number has been assigned to the ultimate rotational compacity, meaning the residual strength would not drop to zero. The building collapse is instead identified as part of the post-processing procedure (see later section).

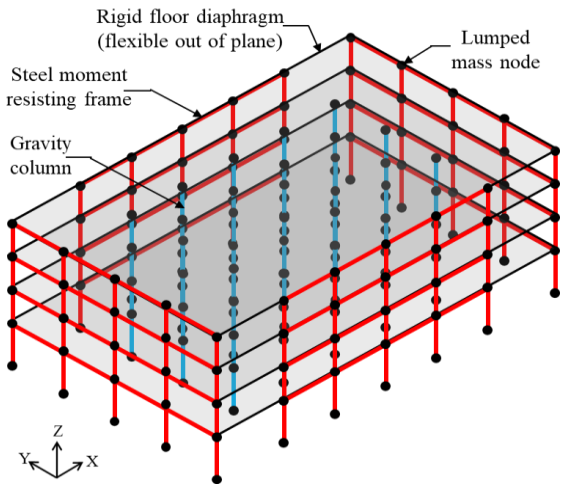

Figure 8: Idealisation of the model of the steel moment resisting frame superstructure.

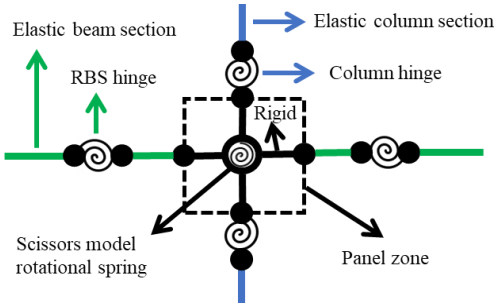

Figure 9: Idealisation of the numerical model of the beam-column-joint with reduced beam section connetcions.

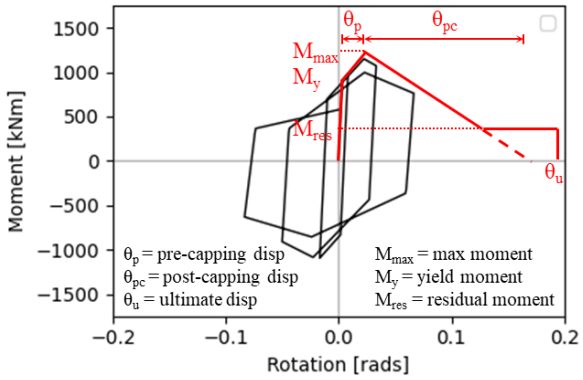

Figure 10: An example of the modified IMK model used to model the RBS hinges and potential column hinges.

The beam-column joints are modelled using the Scissors model, which is a variation of the Krawinkler's Model [40] and first appeared in [41]. Previous study has presented detailed derivations and comparisons of these models [42]. Within the joint region of the Scissors model, the beam and column members are rigid and form a pair of scissors with a rotational spring in the middle, as described in Figure 9. The rotational spring follows a trilinear moment-rotation curve, see Figure 11. The deformation is contributed from the panel zone shear deformation and column flange deformation. The parameters of the rotational spring are estimated using the equations derived by [41,42].

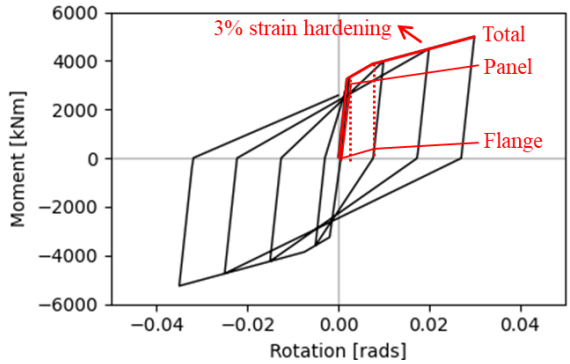

Figure 11: An example of the trilinear hysterstic model used to model the beam-column joint deformation.

The isolation plane is located below the superstructure model, and its components include LRBs, FSs, and grillage beams. The LRB elements have a finite length of around 0.5 m and modelled with six springs; three translational springs and three rotational springs. The two horizontal translational springs are coupled and have a bilinear stress-strain curve, shown in Figure 12. Whereas the rest of the springs are elastic and have realistic stiffness values estimated based on the LRB properties. The FSs also have a finite length that is equal to the LRB height for modelling convenience, and the sliding movement takes place at mid-span. In the horizontal translational direction, the stress-strain behaviour is modelled using a Coulomb friction model with a constant coefficient of friction of 4%. Studies have shown that the coefficient of friction depends on normal stress, velocity, temperature, and other parameters [43]. However, the variation has a minimal impact on the structural response in this study, as the FSs are designed to mostly provide vertical support. The axial stiffness of the FS in compression is assumed to be relatively high such that the axial strain is insignificant. Whereas the axial stiffness in tension and all rotational stiffness are assumed to be zero. As mentioned previously, the isolators are connected by grillage beams, and the building stiffness can be sensitive to the grillage beam stiffness. To capture the flexibility of the grillage beams, they are explicitly modelled using elastic beam-column elements. In addition, the stiffness of the floor slab is also considered by modifying the grillage beam's effective width [22]. The consideration of bearing's deformability in the axial direction and the base level stiffness is an attempt to capture the variation in axial loads due to overturning moment and the transferred axial loads at large displacement due to vertical stiffness incompatibility between the LRBs and FSs, as observed in the experimental test [44].

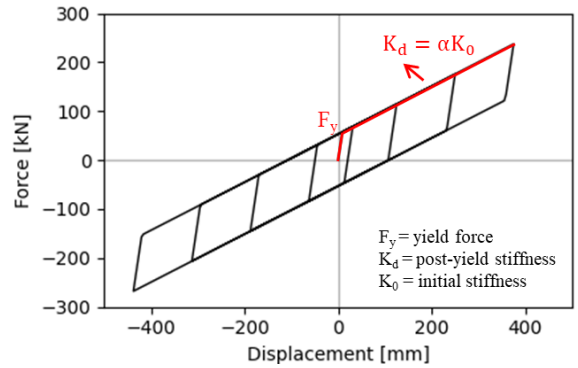

Figure 12: An example of the bilinear hysterstic model used to model the lead rubber bearing.

Pushover Analysis

Nonlinear static analysis (also known as the pushover analysis) is performed to understand the system behaviour of the RC wall and steel MRF models and the possible reasons that may cause different structural responses. As described earlier, each RC wall has a rotational hinge with a 5% strain hardening at the base, whereas for the steel MRFs, there are two hinges assigned to each beam and column. The progressive yielding of all these hinges in the MRF can result in a higher effective stiffness compared to the equivalent RC wall structure, as seen in the example shown in Figure 13. The the base shear shown in Figure 13 is normalised by the self-weight of the superstructure, which is assumed to be the same in this case.

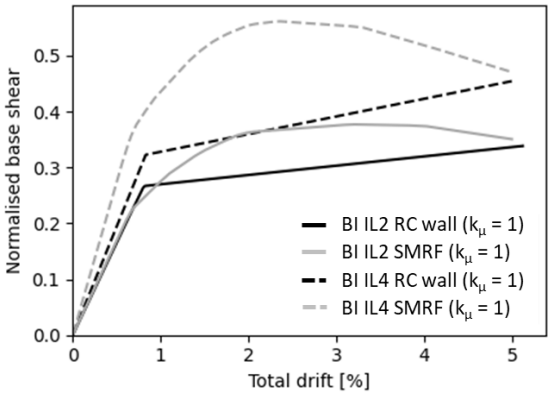

Figure 13: Pushover curves (superstructure only) of the isolated IL2 and IL4 RC wall and steel MRF buildings.

Figure 13 also shows that the IL4 steel MRF has a higher initial stiffness compared to the IL4 RC wall. This is likely a result of the capacity design requirement. Both structural typologies were designed using the same checks reported in Table 2, but to satisfy the capacity design requirements, the columns in the steel MRF were designed to be much stronger, which resulted in a stiffer design. On the other hand, the capacity design requirement in RC wall building is related to the transverse reinforcement, which does not change the flexural strength or stiffness. Therefore, the initial stiffness of the steel MRF structure can sometimes be higher than the RC wall structure.

Non-linear Time History Analysis

The NLTHA are performed using the ground motions described earlier with reference to Table 10. The numerical models are loaded bi-directionally, with no vertical excitation. The equation of motion is solved using the Newmark average acceleration method [45]. The integration time step is initially set to be 0.005s, but if non-convergence is encountered, the time step is automatically reduced to as low as 0.00001s. The norm of the displacement increment is used for a convergence test with a tolerance of 1×10^{-5}. Second order analysis is performed assuming the displacement, rotation, and strain are small compared to the overall structural dimension. The analysis accounts for the second-order P-Δ effects via a linear geometric transformation [46].

The Peak Storey Drift (PSD) and Peak Floor Acceleration (PFA) for all storeys are recorded during the NLTHA. In addition, for base-isolated buildings, the maximum isolator displacement (combined from orthogonal directions) is also recorded. An example of the PSD of the base-isolated RC IL2 building is presented in Figure 14. A lognormal distribution is fitted to results at each intensity to obtain the median and dispersion values. Note that if the building collapsed, its structural response is not included when calculating the median, this is because some of the collapsed results have extremely large values due to numerical issues. When more than 50% of

cases collapsed at an intensity, the median value is less representative of the trend in total median demands, and is therefore not shown.

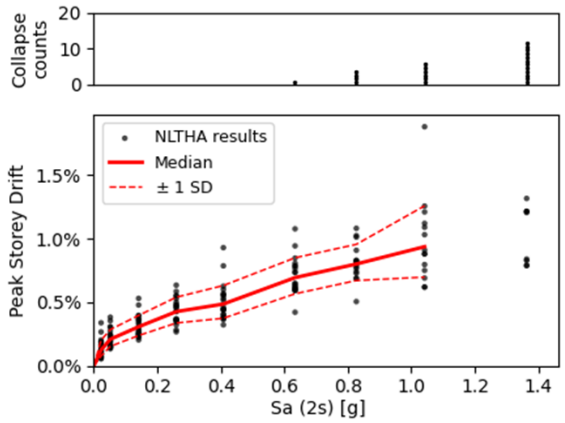

Figure 14: An example of the processed multi-stripe analysis results (median and dispersion are conditioned on non-collapse).

Collapse Analysis

At large shaking intensities, excessive building deformation can cause damage that is not repairable and could result in building collapse. In this study, buildings are thought to collapse when either the superstructure or the isolators have reached their maximum deformation capacity. For the steel MRF structure, superstructure collapse is defined by the fracture of the reduced beam section or column failure. The fragility functions for such damage states have been investigated in a number of studies. The constitutive model used to model RBS hinges in this study recommends an ultimate rotation of 5 % to 6% [38]. However, this estimation varies largely depending on the loading history. FEMA P-58-3 recommended a median storey drift ratio of 5.3% with a dispersion of 0.3, or a beam plastic hinge rotation of 4.7% with a dispersion of 0.3 [47]. Another study recommended a median storey drift of 5.0% with a dispersion of 0.31, or a joint plastic rotation of 4.1% with a dispersion of 0.37 [48]. Based on the available information provided in the literature and available results from the NLTHA, the beam plastic hinge rotation capacity is assumed to have a median value of 4.7% and a dispersion of 0.3. In addition, a 10% storey drift limit is imposed to capture the column failure at the base. Recall that the steel MRFs are capacity designed and will develop a strong column-weak beam failure mechanism.

For the RC wall structure, superstructure collapse occurs when the drift demand calculated from roof displacement exceeds the ultimate wall drift capacity, which is defined as the roof displacement at which the wall strength degrades to 80% of its peak strength. Equation (3) is used to estimate the drift capacity for walls with boundary elements [49].

$$\frac{\delta_c}{h_w}(\%) = 3.85 - \frac{\lambda_b}{\alpha} - \frac{v_{max}}{0.83\sqrt{f_c' MPa}} \quad (3)$$

Where λ_b is the ratio of the neutral axis depth to compression zone width multiplied by the ratio of the wall length to compression zone width; α considers the configuration of the transverse reinforcement within the boundary elements; v_{max} is the maximum shear stress; and f_c' is the concrete compressive strength. For the shorter walls in the X-direction (around 3m long), the wall drift capacities are 3.5% to 3.8%. For the longer walls in the Y-direction (around 6m long), the wall drift capacities are 1.7% to 2.7%. The value estimated using Equation (3) is treated as the median drift capacity with an assumed dispersion of 0.3. It is worth noting that the collapse definitions for both steel MRFs and RC walls may be conservative, and there could still be residual strength in the buildings after a RBS fracture or a 20% drop in peak strength. However, the relative comparisons of the building performance are likely to hold and the conclusions made in this paper about relative performance should not be impacted.

In addition to the superstructure, the failure of the lead rubber bearing isolators occurs when the shear strain exceeds a threshold. The shear strain of the LRB is defined as the horizontal displacement normalised by the total thickness of the rubber layers. Experimental test results related to the ultimate shear strain of LRBs are limited and show a large variation [50-57]. Therefore, the fragility function of the LRB is assumed to have a 5th percentile of 250% shear strain (equivalent to 630mm), as this is the design limit recommended by the NZSEE guidelines. Together with an assumed dispersion of 0.3, the median shear strain capacity is calculated to be 410% (equivalent to 1033mm). Future research should aim to generate more data to support or update this number.

Compute Collapse Fragility Function and Annual Collapse Rate

In the previous section, the collapse conditions of the case study buildings were defined. In this section, the method used to develop building fragility functions and collapse rates is presented. The annual rate of collapse (λ_c) is computed using Equation (4).

$$\lambda_c = \int_{IM_0}^{IM_\infty} P(collapse|IM = x) \cdot |d\lambda_{IM}(IM > x)| \quad (4)$$

Where $P(collpase|IM = x)$ is the collapse fragility function which describes the probability of collapse at a given intensity, $IM = x$. The term $|d\lambda_{IM}(IM > x)|$ is the derivative of the ground motion hazard curve and provides the rate of occurrence of the ground motions with intensities between x and $x + dx$ [58]. $[IM_0, IM_\infty]$ is the analytical integration domain. IM_0 is defined such that the collapse probability below this intensity is small so that it has a negligible impact on the annual collapse rate. Similarly, IM_∞ is defined such that the rate of occurrence beyond this intensity is sufficiently small that it has a negligible impact on the annual rate of collapse.

The collapse fragility function is developed using the Maximum Likelihood method. For NLTHA results, the probability of observing z_i collapses out of n_i ground motions at each intensity level can be modelled using the binomial distribution, assuming the collapse is independent between each ground motion. The product of these binomial probabilities gives the likelihood for the data set. The Maximum Likelihood method can be applied to find a median (θ_c) and a dispersion (β_c) to a lognormal distribution such that provides the highest likelihood of producing the observed data set [59].

Uncertainty Treatment

There are uncertainties associated with each step of the analysis. For example, FEMA P-58-1 suggests that the modelling uncertainty (β_m) is associated with the quality of the analytical model (β_q) and level of building definition and construction quality assurance (β_c) [24]. Assuming an average quality analytical model ($\beta_q = 0.25$) and a high construction quality assurance ($\beta_c = 0.1$), the overall modelling uncertainty is $\beta_m = \sqrt{0.25^2 + 0.1^2} = 0.27$. The record-to-record variability (β_{rtr}) in ground motions is accounted for by using multiple sets of ground motions. There are also uncertainties associated with the assumed building capacity, as alluded to earlier when defining the collapse conditions.

The β_m and β_{rtr} can be combined using the Root Sum Square (RSS), under the assumptions that they are independent, and their distributions are lognormal. However, recall that collapse

is multicriteria, and therefore the uncertainties in the superstructure and isolation plane capacities cannot be directly combined using RSS. Instead, Monte Carlo simulation is used to combine the uncertainties in capacities, where 500 samples are randomly generated from each capacity distribution. For each generated capacity, summing up the collapse counts and divided by the number of trials gives the probability of collapse at each intensity.

Loss Assessment

The loss assessment is carried out using the Performance Assessment Calculation Tool (PACT) provided in FEMA P-58-3 [60]. To perform loss analysis, a building performance model must be constructed first. Note that in this study, only direct repair cost is considered in the loss assessment, other secondary losses such as downtime and carbon footprint are not included.

The building performance model in PACT requires the basic building information such as dimensions, number of storeys, building initial cost, and replacement cost. The initial building cost is estimated based on simplified square meter rates and does not account for the differing costs associated with different structural systems and elemental weights. The rates from Rawlinson's Construction Handbook [61] for Wellington region are adopted. In this study, the case study buildings are assumed to be office buildings. The building cost for a traditional fixed-base building in year 2023 (adjusted for inflation) of this size is $10.8 million NZD including the base building cost and standard fit out cost. It is assumed that the base isolation design would add 5% to the building cost, which includes the costs of the isolation devices, consultancy, testing, and installation. This brings the building cost of the base-isolated building to $11.4 million NZD. FEMA P-58-1 recommends a replacement cost of 125% of the building value which includes demolition and site clearance [24]. In line with the above, the replacement costs for the fixed-base building and base-isolated building are $13.5 million and $14.2 million NZD, respectively. FEMA P-58-1 also recommends a loss threshold of 50% of the replacement cost, as studies show that owners are likely to replace the building when the repair costs exceed this loss threshold [24]. The last piece of information required to complete the building performance model is the list of damageable structural and non-structural components and their quantities, component fragility functions, and consequence functions. The buildings in this study adopt the architectural design for an office building from a previous study [20], [62]. The damageable components and the reference to the fragility and consequence functions used in this work are listed in Table 11. Note that all repair costs have been adjusted for inflation to the year 2023.

In addition to the performance model, PACT requires a few inputs to complete the loss analysis, including the hazard curve, NLTHA results (e.g. PSD, PFA, and isolator displacement) at each intensity, and the collapse fragility. All of the inputs have been introduced in the previous sections. 500 realisations are generated in PACT, the repair costs of every component at every intensity level are recorded.

Computation of Building Loss Function

With the loss results generated from PACT, one can compute a building loss function, also referred to as the vulnerability function. This describes the relationship between the repair cost and the intensity measure. An example is presented in Figure 15. Assuming each realisation has the same weight, the expected repair cost at each intensity is equal to the average value. The loss function is linearly interpolated between each intensity level. The probability densities of the realisations are also plotted in Figure 15 at the return periods of 2475 years and 9975 years, respectively. Noting that there are a significant number of realisations that reached 100% replacement cost at higher intensities, as they either exceeded the 50% loss threshold or caused collapse.

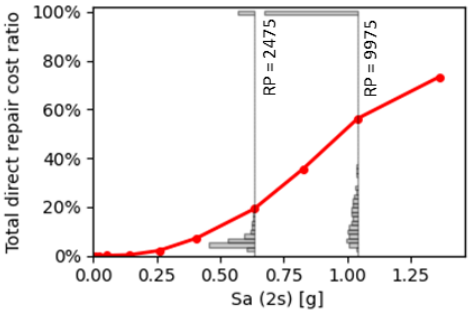

Figure 15: The loss function of the IL2 base-isolated RC wall buidling.

Table 11: Summary list of repairable components included in the loss assessment.

Repairable components	Fragility functions	Cost functions
Structural components		
RC structural wall	[63]	[64]
Steel RBS connections	[48]	[64]
Column base	*	*
Drift sensitive non-structural components		
Full-height partitions	[65]	[64]
Partial-height partitions	[65]	[64]
Interior glazing	*	*
Exterior glazing	*	*
Precast stairs	*	[64]
Acceleration sensitive non-structural components		
Suspended ceiling	*	[64]
Independent pendant lighting	*	*
Air handling units	*	*
Traction elevator	*	*
Water piping & bracing	*	*
Sanitary waste piping & bracing	*	*
Chiller capacity	*	*
Ducts	*	*
Droppers and diffusers	*	*
Coils	*	*
VAV boxes	*	*
Fire sprinkler pipes	*	*
Fire sprinkler drops	*	*
Transformers	*	*
Cooling tower capacity	*	*

** PACT default fragility library (FEMA-P-58-3)* [60]

Computation of Expected Annual Loss

The Expected Annual Loss (EAL) can be computed using Equation (5).

$$E[C] = \int_{IM_0}^{IM_\infty} E[C|IM = x] \cdot |d\lambda_{IM}(IM > x)| \qquad (5)$$

The notation C stands for consequence, which in this case represents the direct repair cost. $E[C|IM = x]$ is the loss function described in Figure 15. $d\lambda_{IM}(IM > x)$ is the rate of occurrence of the ground motions with intensities between x and $x + dx$, as explained in Equation (4). With knowledge of the loss function and hazard curve, one can therefore compute

the EAL. Furthermore, Equation (5) also provides insight into which IM levels contribute most to the EAL.

IMPACTS OF SUPERSTRUCTURE DESIGN DUCTILITY AND BUILDING IMPORTANCE LEVELS

Recall that there are 16 case study buildings in total, apart from the four fixed-base buildings, the rest are base-isolated buildings with different superstructure inelastic-spectrum-scaling factors ($k_\mu = 1$ and $k_\mu = 2$) and importance levels (IL = 2 and IL = 4). This section will discuss the impacts of these variables on building performance in terms of the structural response parameters, collapse fragility, annual rate of collapse; loss function, and expected annual loss. Furthermore, the impact of imposing a drift limit of 0.5% at the DCLS as a means of damage control is also investigated (referred to as $k_\mu = 2$ DC in the following sections).

Structural Response

The median structural response including the PSD, PFA, and maximum LRB shear strain demands are presented in Figures 16 to 18, respectively. The shear strain is computed by normalising the LRB displacement by the total rubber thickness. The LRB displacement is computed by combining the displacements in the orthogonal directions at each timestep of the analysis. The key return periods that correspond to the design limit states (e.g. SLS1/2, DCLS, ULS, and CALS) are highlighted. The median values are conditioned on the non-collapsed cases and are less indicative of the likely response at higher intensities, due to fewer points being available.

Comparing the PSD demands between the base-isolated structures with $k_\mu = 1$ and $k_\mu = 2$ in Figures 16a and 16b. It is observed that by permitting a higher k_μ, the PSD demands increased by around 50% to 100% across all design intensity levels. This result is expected, as the higher inelastic-spectrum-scaling factor is likely to result in a more flexible superstructure design. Interestingly, the more flexible superstructure design did not reduce the PFA demands, as suggested by Figures 17a and 17b. Similar results were observed [66], showing that a base-isolated braced frame building that had a higher design ductility reduced the PFA by just 20% but increased the PSD by up to 75%. Comparing the maximum LRB shear strain in Figures 18a and 18b, again, a higher k_μ did not affect the peak LRB displacement demands at intensity levels lower than 0.6g. The differences in LRB shear strain become more apparent at higher intensity levels, possibly due to the superstructure yielding. The $k_\mu = 2$ DC scenario with a drift limit at the DCLS appeared to effectively reduce the PSD demands in most of the case study buildings.

Considering the impact of the importance level, it is observed that designing base-isolated buildings with a higher IL does not necessarily reduce the PSD demands. For example, comparing the PSD demand of the IL4 RC wall ($k_\mu = 1$) to that of the IL2 RC wall ($k_\mu = 1$) in Figure 16, it is seen that the IL4 building has higher PSD demand. Another example is to compare the IL4 RC wall ($k_\mu = 2$) with the IL2 RC wall ($k_\mu = 2$). The PSD demands are similar at low intensities and a reduction in demand only becomes more significant at higher intensities due to the yielding of the IL2 RC wall. The observation above may be explained by the higher base shear demands experienced by the stiffer and stronger isolators in the IL4 buildings, recalling from Table 4 that the IL4 buildings were all provided with almost twice the base shear strength of the IL2 buildings. The IL4 steel MRF buildings are noticeably stiffer than the IL4 RC wall buildings, which is likely due to the capacity design requirement and post-yield stiffness as explained in Figure 13. The higher base shear demands in the IL4 buildings also led to a 50% ~ 60% increase in PFA demands, as shown in Figures 18a and 18b. The amount of increase in PFA appears to be affected by the stiffness of the isolation system. Increasing the deign importance level has mixed effects on the maximum LRB shear strain demands. The shear strain demands would increase due to the higher base shear but decrease because of the stiffer isolators.

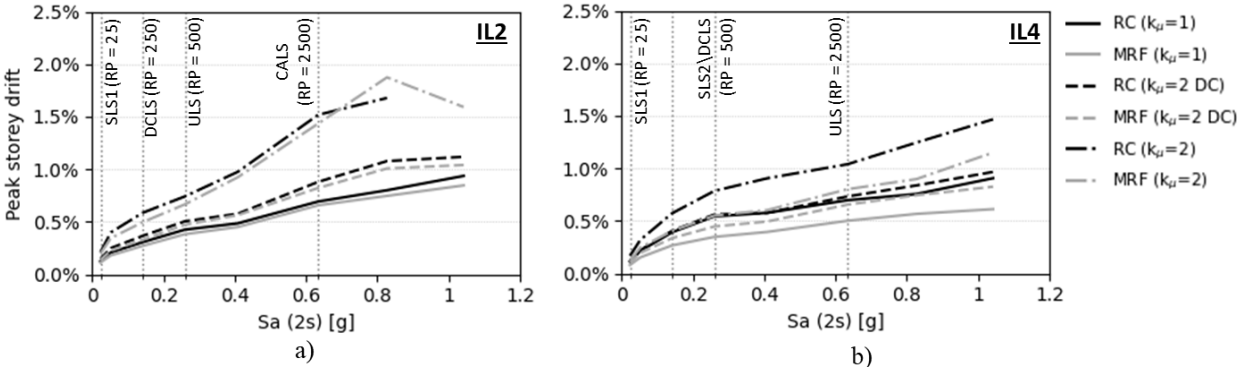

Figure 16: The peak storey drift demand (median values) in the base-isolated buildings, a) IL2 buildings and b) IL4 buildings.

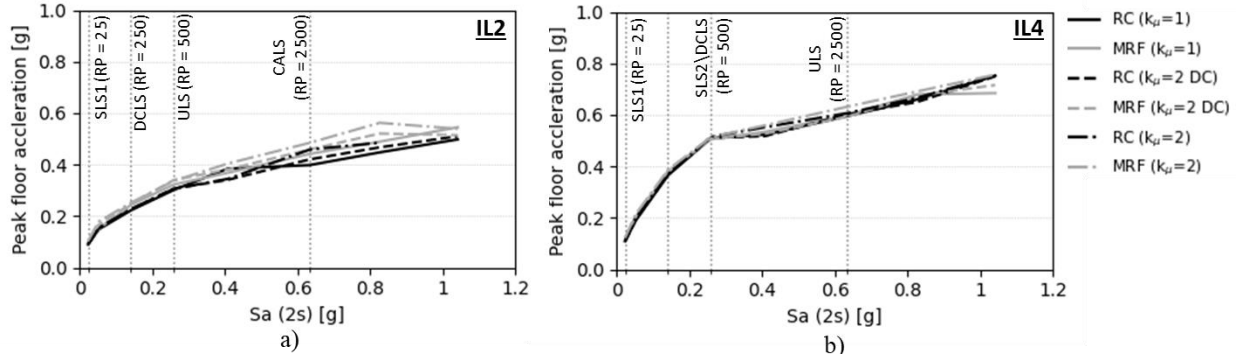

Figure 17: The peak floor accleration demands (median values) in the base-isolated, a) IL2 buildings and b) IL4 buildings.

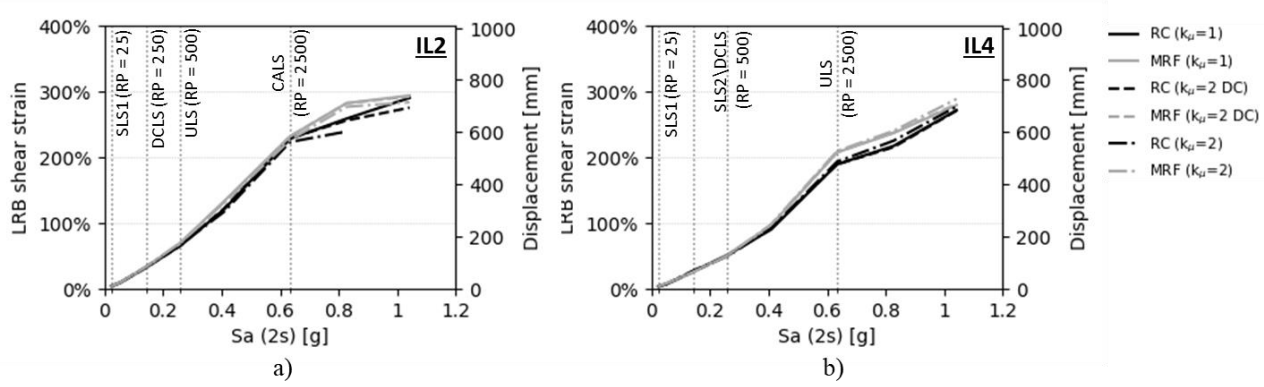

Figure 18: The maximum isolator shear strain demands (median values) in the base-isolated buildings, a) IL2 buildings, and b) IL4 buildings.

Collapse Performance

The base-isolated building collapse is associated with the failure in the superstructure or in the isolation system and is sensitive to the definition of the collapse criteria. Recall that in this study, the RC wall failure is related to roof displacement, the steel MRF failure is related to beam plastic hinge rotation, and the isolation system failure is related to LRB shear strain. The annual rates of collapse of all case study buildings are compared in Figure 19 and the values are reported in Table 12. The collapse results show that the annual rates of collapse of the IL2 base-isolated buildings are around 1.8 to 2.7 × 10^{-4}. Whereas the collapse rates of the IL4 base-isolated buildings are on average halved, around 1.1 to 1.4 × 10^{-4}. Better collapse performance in IL4 buildings is expected because of the higher structural deformation capacity in RC walls and reduced PSD demands in steel MRFs.

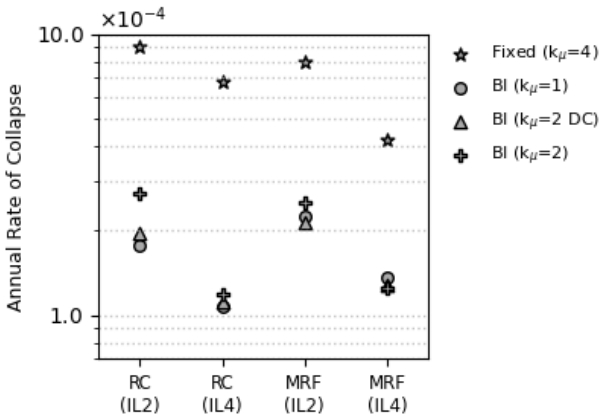

Figure 19: The annual rate of collpase of all case study buidlings located in Wellington.

Table 12: The annual rate of collapse, λ_c (× 10^{-4}) of the case study buildings located in Wellington.

Design Scenario	RC IL2	RC IL4	MRF IL2	MRF IL4
Fixed-base	9.0	6.8	8.0	4.2
BI $k_\mu = 1$	1.8	1.1	2.2	1.4
BI $k_\mu = 2$ (DC)*	2.0	1.1	2.1	1.3
BI $k_\mu = 2$	2.7	1.2	2.5	1.3

** Design scenario where an additional drift limit (0.5%) is imposed at the DCLS*

To better understand the isolated building failure mechanism and the impacts of the inelastic-spectrum-scaling factor and the importance level on the collapse performance, the individual collapse fragility curves for the superstructure and the isolator may be considered separately. For instance, the superstructure collapse fragility function can be estimated by disregarding the isolator failure (i.e. by assuming it has enough displacement capacity), and vice versa. The system collapse fragility curve is the envelope of the two separate fragility curves. An example of the three base-isolated IL2 RC wall buildings are plotted in Figure 20. The medians (θ) and dispersions (β) of the fragility curves are also reported.

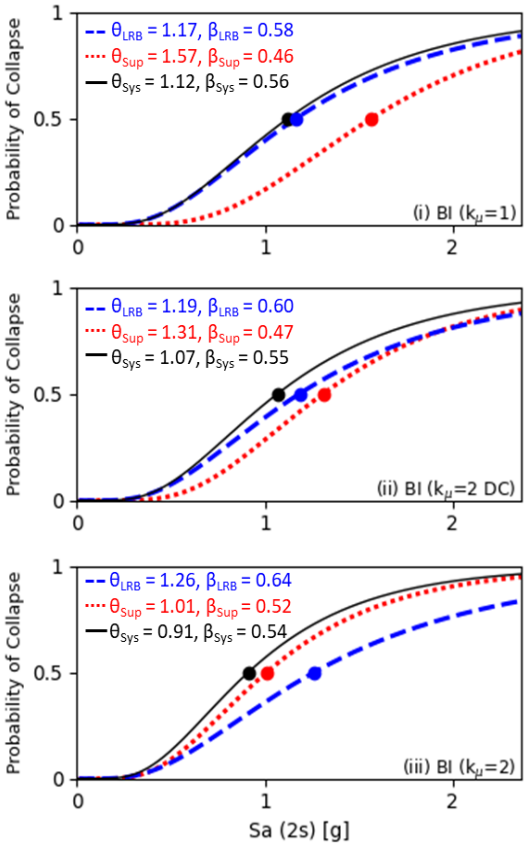

Figure 20: Collapse fragility curves for the IL2 base-isolated RC wall building with superstructure inelastic-spectrum-scaling factors of $k_\mu = 1$, $k_\mu = 2$ (0.5% drift limit at DCLS), and $k_\mu = 2$.

Among the three case study buildings in Figure 20, the RC wall building with $k_\mu = 1$ has the highest stiffness whereas the design with $k_\mu = 2$ has the lowest stiffness. As the superstructure stiffness reduces, the superstructure collapse median is reduced as a result of increased PSD demands, as shown previously in Figure 16a. The LRB collapse median does not seem to be significantly affected, which again matches the observation in

Figure 18a, where the LRB shear strain appears to be unaffected by the change of k_μ. The shifting of the superstructure collapse fragility curve can sometimes result in a change of failure mechanism, as seen in Figure 20. Note that moat wall impact is not included in the scope of this study. The impact can amplify the superstructure demands depending on a few factors such as stiffness of the contact elements, impact speed, etc. This may affect the collapse performance of the base-isolated buildings and should be investigated as part of future research. One option to improve the collapse performance of base-isolated buildings is to provide additional isolator displacement capacity given the superstructure is designed with $k_\mu = 1$. If a higher k_μ is adopted, then the designer should consider applying a drift limit at the DCLS to ensure the superstructure is sufficiently stiff to properly benefit from the isolation devices.

Loss Performance

The total EALs of all base-isolated case study buildings are reported in Table 13. The loss is due to contributions from acceleration-sensitive non-structural components, drift-sensitive non-structural components, structural components, and building replacement. The latter three are related to drift because the building replacement is mostly induced by building collapse, which is triggered when a certain deformation limit is exceeded. Table 13 suggests that the isolated buildings with $k_\mu = 2$ on average experienced 60% higher EALs compared to those with $k_\mu = 1$. The higher losses are mostly associated with increased damage to the drift sensitive non-structural and structural components (see Figure 21). Imposing a 0.5% drift limit at the DCLS design intensity seems to have effectively controlled the damage, as the EALs of the buildings with $k_\mu = 2$ (DC) were similar to those with $k_\mu = 1$.

Table 13: The total expected annual loss values of all case study buildings.

	RC IL2	RC IL4	MRF IL2	MRF IL4
Fixed-base	0.290%	0.239%	0.276%	0.207%
BI $k_\mu = 1$	0.045%	0.051%	0.043%	0.037%
BI $k_\mu = 2$ (DC)*	0.042%	0.053%	0.049%	0.041%
BI $k_\mu = 2$	0.088%	0.076%	0.073%	0.049%

** Design scenario where an additional drift limit (0.5%) is imposed at the DCLS*

Comparing the IL4 to the IL2 base-isolated buildings in Figure 21, the contribution from the acceleration-sensitive components is increased, and the contribution from building collapse is reduced. This matches with the previous observation of increased PFA demands and reduced collapse rates in IL4 buildings. The loss estimation of the IL4 buildings may be slightly conservative, as all case study buildings share the same non-structural element fragility library, but some of the non-structural elements (e.g. braced elements) in the IL4 buildings could have higher capacities to comply with the design requirements. Future research will aim to update the component fragility library to reflect this difference. Overall, the results suggest that designing a base-isolated building with a higher importance level could reduce the EAL, but the amount will depend on the type and quantity of the acceleration- and drift-sensitive non-structural components.

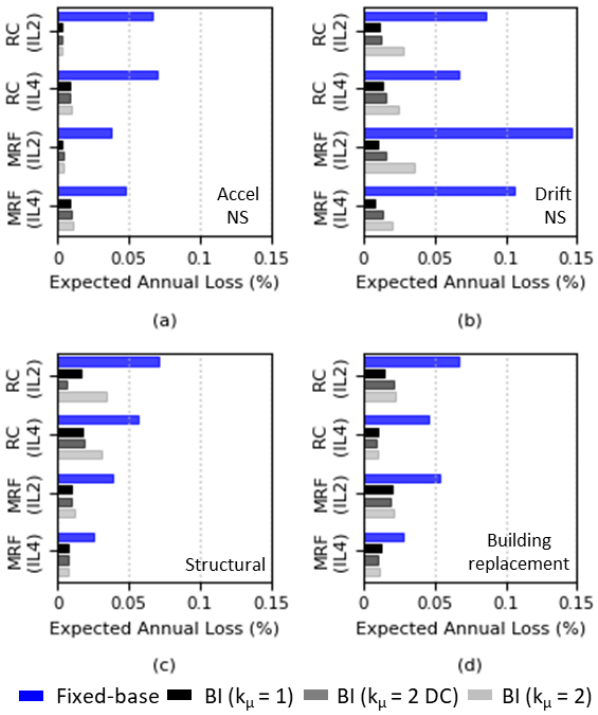

Figure 21: A comparison of the EAL contributions from a) acceleration sensitive non-structural components, b) drift sensitive non-structural components, c) structural components, and d) building replacement.

The loss functions of the base-isolated buildings are plotted in Figure 22. The total repair cost increases with the intensity measure in a trend that appears to be somewhat bilinear. According to Figure 22, at a given shaking intensity, the IL4 buildings on average cost less to repair compared to the IL2 buildings. However, at a given limit state, the IL4 buildings experienced higher losses compared to the IL2 buildings. For instance, the repair cost ratios at the ULS for IL4 buildings are around 20%, whereas the repair cost ratios for IL2 buildings are around 5 to 10%. This would suggest that the building loss performance is slightly inconsistent across different importance levels.

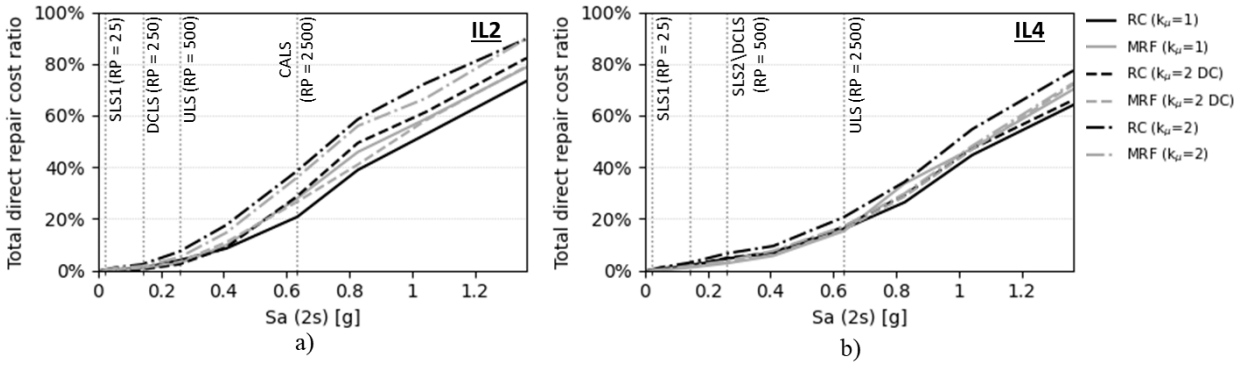

Figure 22: A comparison of the loss functions obtained for base-isolated case study buildings.

COMPARING PERFORMANCE OF BASE-ISOLATED BUILDINGS TO FIXED-BASE BUILDINGS

This section will discuss the performance of the base-isolated buildings compared to fixed-based buildings. The building performance in terms of structural response, annual rate of collapse, and loss due to direct repair costs are discussed. The comparison of median PSD demands is plotted in Figure 23. Note that the demands are plotted against the return period instead of spectral acceleration for the convenience of comparing the fixed-base buildings with base-isolated buildings, because their NLTHA results are conditioned on different intensity measures (i.e. Sa (1.0s) and Sa (2.0s)). At the ULS shaking intensity, the PSD demands for IL2 fixed-base buildings are around 2% to 2.5%, whereas for IL4 fixed-base buildings they have reached 3.5% and exceed the design drift limit. The unconservative results may be explained by the underestimation of the rates of higher intensity earthquakes in the current design code [15], as suggested by Figure 5. In comparison, the PSD demands for base-isolated buildings have reduced to between 0.5% and 1%.

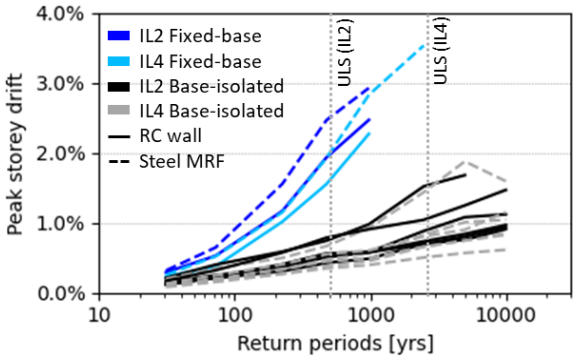

Figure 23: A comparison of the peak storey drift between the fixed-base and isolated buildings.

The comparison of median PFA demands between the base-isolated and fixed-base buildings is plotted in Figure 24. At the ULS shaking intensity, the PFA demands for IL2 fixed-base buildings are around 0.8g to 1.3g, and for IL4 fixed-base buildings the demands are 1.3g to 1.6g. The PFA demands have reduced to 0.3g and 0.6g for the IL2 and IL4 base-isolated buildings, respectively. The comparisons suggest that the base-isolated buildings have better performance in terms of structural responses.

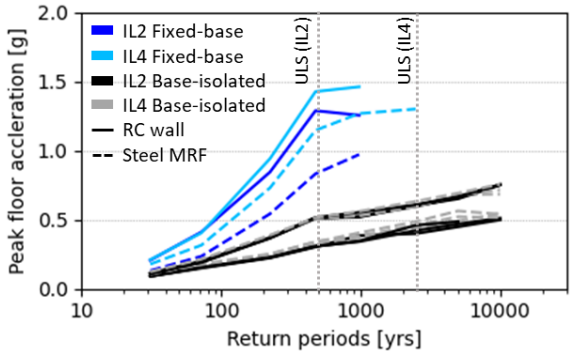

Figure 24: A comparison of the peak floor accleration between the fixed-base and isolated buildings.

The annual rates of collapse of the fixed-base buildings were previously plotted in Figure 19 and reported in Table 12. The IL2 fixed-base buildings have the highest annual rate of collapse which on average is 8.5×10^{-4}, followed by the IL4 fixed-base buildings with an average of 5.5×10^{-4}. With base isolation, the average annual rates of collapse of IL2 and IL4 base-isolated buildings are reduced to 2.2×10^{-4} and 1.2×10^{-4}, respectively. The EALs of the fixed-base buildings were reported in Table 13 and the breakdown of component contributions were plotted in Figure 21. The average EALs are 0.28% and 0.22% for the IL2 and IL4 fixed-base buildings, respectively. In comparison, the average EALs are 0.06% and 0.05% for the IL2 and IL4 base-isolated buildings, respectively. The above comparisons demonstrate that base isolation can effectively reduce the annual rate of collapse and expected annual loss by a factor of four.

The loss functions of the fixed-base buildings and base-isolated buildings are plotted in Figure 25. It can be seen that the total direct repair costs for the fixed-base buildings start to depart from zero at a return period of around 75 years, whereas the increase in total direct repair cost for base-isolated buildings is not observed until around 250 years. This suggests that the base-isolated buildings are less likely to experience damage under low to moderate intensity earthquakes.

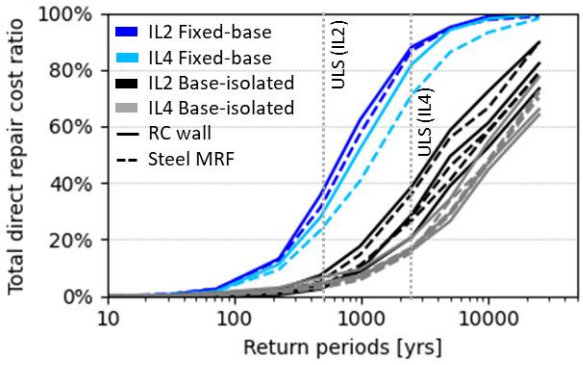

Figure 25: A comparison of the loss functions obtained for fixed-base and base-isolated buildings.

CONCLUSIONS

This study investigated the performance of base-isolated buildings designed following the recommendations provided in the NZSEE/MBIE base isolation design guidelines. This work was motivated by observations internationally [8] that base-isolated buildings may not perform well relative to other building typologies without suitable design provisions, whilst also recognising that the NZSEE/MBIEs guidelines have not undergone significant testing to date. The performance of the case study buildings was assessed by following the FEMA P-58 framework [24], and by examining values of peak storey drift, peak floor acceleration, maximum isolation displacement, annual rate of collapse, and expected annual loss. Comparisons were made between the isolated buildings and traditional fixed-base buildings. In addition, the impacts of permitting a higher superstructure design ductility (controlled via the inelastic-spectrum-scaling factor, k_μ) and a higher importance level were also investigated.

In total 16 case study buildings were designed for a site in Wellington, New Zealand. The buildings can be divided into four groups; RC wall (IL2), RC wall (IL4), steel MRF (IL2), and steel MRF (IL4). Within each group, there were four building designs, including a fixed-base building and three base-isolated buildings with $k_\mu = 1$, $k_\mu = 2$ (0.5% drift limit at DCLS), and $k_\mu = 2$. All buildings were four storeys tall and possessed the same architectural layout assuming office buildings. The isolation plane consisted of lead rubber bearings in combination with flat sliders.

Three-dimensional numerical models were constructed in OpenSees, and NLTHAs were performed using 180 ground motions at nine intensity levels. Results showed that:

- The collapse and loss performance of the isolated buildings (designed using S_p = 1) was superior compared to the traditional fixed-base buildings. The PSD demands were reduced by up to five times and the PFA demands were reduced by up to three times. The average annual rate of collapse of the fixed-base building was found to be four times higher than the base-isolated buildings (rates of 5.5 to 8.5 × 10^{-4} versus 1.2 to 2.2 × 10^{-4}, respectively). The average EAL of the fixed-base buildings was also found to be four times that of the base-isolated buildings (EAL values of 0.22% to 0.28% and 0.05% to 0.06% of the building replacement cost, respectively).
- A higher superstructure k_μ in a base-isolated building tended to worsen the relative performance. Increasing k_μ from one to two (and maintaining S_p = 1 in both designs) increased the PSD demands by 50% ~ 100% and did not reduce the PFA demands. As a result, the EAL was higher due to the increased damage in drift sensitive non-structural and structural components. In terms of collapse performance, it was observed that the failure mechanism was governed by isolator failure with $k_\mu = 1$. But with an increase in k_μ, the superstructure fragility curve shifted to the left and sometimes governed the system failure mechanism, resulting in a higher annual rate of collapse.
- Imposing a drift limit of 0.5% as part of a damage control limit state check for the design of isolated buildings with a $k_\mu = 2$ proved to reduce the EAL, compared to the equivalent buildings without the drift limit. The design results showed that imposing a drift limit tends to reduce the superstructure design ductility, which again highlights the conclusion that a lower superstructure k_μ can produce a better performance, provided the building is detailed with good ductility.
- In this work, the IL4 base-isolated buildings were designed with stiffer and stronger isolators and superstructure compared to the IL2 buildings, in response to the higher design seismic demands. Subsequently, the IL4 isolated buildings experienced higher base shear which led to a 50% to 60% increase in PFA demands. The PSD demands increased with the higher base shear but reduced due to the stiffer superstructure, thus, the overall PSD demands may or may not be reduced. On average the annual rate of collapse of IL4 isolated buildings was 50% lower compared to the IL2 ones, as a result of the higher structural deformation capacity in RC walls and reduced PSD demands in steel MRFs. The average EALs of IL4 and IL2 buildings were similar and are likely to be sensitive to the type of building usage (i.e. non-structural component types and quantities).

REFERENCES

1 Stanton J and Roeder C (1991). "Advantages and limitations of seismic isolation". *Earthquake Spectra*, **7**(2): 301–324. http://dx.doi.org/10.1193/1.1585630

2 Skinner RI, Robinson WH and McVerry GH (1993). *An Introduction to Seismic Isolation*. ISBN 10: 047193433X John Wiley and Sons, Chichester, UK and New York, 354 pp. https://doi.org/10.1111/j.1475-1305.1993.tb00842.x

3 Christopoulos C and Filiatrault A (2006). *Principles of Passive Supplemental Damping and Seismic Isolation*. 1st Edition, ISBN-10: 8873580378. IUSS Press, 480pp.

4 American Society of Civil Engineers (2021). "*Minimum Design Loads and Associated Criteria for Buildings and Other Structures: ASCE/SEI 7-22*". American Society of Civil Engineers. https://doi.org/10.1061/9780784415788

5 Europena Committee for Standarization (2004). "*Eurocode 8: Design of Structures for Earthquake Resistance – Part 1: General Rules, Seismic Actions and Rules for Buildings"*. British Standards Institution, London.

6 MBIE (2023). "*New Zealand Building Regulations 1992*". Ministry of Business, Innovation and Employment, Wellington. https://www.legislation.govt.nz/regulation/public/1992/0150/latest/whole.html#DLM164788

7 NZSEE/MBIE (2019). "*Guideline for the Design of Seismic Isolation Systems for Buildings*". New Zealand Society of Earthquake Engineering. https://www.nzsee.org.nz/wp-content/uploads/2019/06/2825-Seismic-Isolation-Guidelines-Digital.pdf

8 Iervolino I, Spillatura A and Bazzurro P (2018). "Seismic reliability of code-conforming Italian buildings". *Journal of Earthquake Engineering*, **22**(2): 5–27. https://doi.org/10.1080/13632469.2018.1540372

9 Yang A (2020). "*Seismic Performance Assessment of a Base Isolated Building*". Master Thesis, University of Canterbury, Christchurch, New Zealand, 219pp. https://ir.canterbury.ac.nz/items/52d8770d-d1d3-4c3c-93a7-cdd80c37e3d4

10 Cutfield M (2015). "*Advanced Methods for Performance-Based Seismic Loss Assessment and Their Application to A Base Isolated and Conventional Office Building*". PhD Dissertation, University of Auckland, Auckland, New Zealand, 291pp. https://researchspace.auckland.ac.nz/docs/uoa-docs/rights.htm

11 Bustamante R, Mosqueda G and Elwood KJ (2021). "Moat wall pounding analysis for a prototype base-isolated building". *Structural Engineering Society (SESOC) New Zealand Conference*, July 5-6, Hamilton, New Zealand. https://2021conf.sesoc.org.nz/PDFs/S1%20Plenary%20P4%20-%20Elwood_Bustamante_Mosqueda.pdf

12 Cong Z, Chase G, Rodgers G, Kuang A, Gutschmidt S and Xu C (2015). "Performance evaluation of CWH base isolated building during two major earthquakes in Christchurch". *Bulletin of the New Zealand Society for Earthquake Engineering*, **48**(4): 264–273. https://doi.org/10.5459/bnzsee.48.4.264-273

13 Gavin HP and Wilkinson G (2010). "Preliminary observations of the effects of the 2010 Darfield earthquake on the base-isolated Christchurch Women's Hospital". *Bulletin of the New Zealand Society for Earthquake Engineering*, **43**(4): 360–367. https://doi.org/10.5459/bnzsee.43.4.360-367

14 Pettinga D (2018). "*Detailed Seismic Assessments for Christchurch Women's Hospital and Clinical Services Building*". Report prepared for Canterbury District Health Board, Report ID: CDHB 9873, Canterbury, New Zealand, 236pp. https://www.cdhb.health.nz/about-us/document-library/detailed-seismic-assessments-for-christchurch-womens-hospital-and-clinical-services-building/

15 Standards New Zealand (2016). "*NZS 1170.5:2004 Structural Design Actions - Part 5: Earthquake Actions – New Zealand"*. Standards New Zealand, Wellington, New Zealand, 76pp. https://www.standards.govt.nz/shop/nzs-1170-52004/.

16 Standards New Zealand (2011). "*AS/NZS 1170.0:2002 Structural Design Actions – Part 0: General principles*". Standards New Zealand, Wellington, New Zealand, 42pp. https://www.standards.govt.nz/shop/asnzs-1170-02002/

17 McVerry GH, Zhao JX, Abrahamson NA and Somerville PG (2006). "New Zealand acceleration response spectrum attenuation relations for crustal and subduction zone earthquakes". *Bulletin of the New Zealand Society for Earthquake Engineering*, **39**(1): 1-58. https://doi.org/10.5459/bnzsee.39.1.1-58

18 Freeman S (1978). "Prediction of response of concrete buildings to severe earthquake motion". *Douglas McHenry International Symposium on Concrete and Concrete Structures*", Publication SP-55, American Concrete Institute, Detroit, Michigan, U.S.A.

19 American Society of Civil Engineers (2017). "*Minimum Design Loads and Associated Criteria for Buildings and Other Structures: ASCE/SEI 7-16*". American Society of Civil Engineers. https://doi.org/10.1061/9780784414248

20 Yeow TZ, Orumiyehei A, Sullivan TJ, MacRae GA, Clifton GC and Elwood KJ (2018). "Seismic performance of steel friction connections considering direct-repair costs". *Bulletin of Earthquake Engineering*, **16**(12): 5963–5993. https://doi.org/10.1007/s10518-018-0421-x

21 Priestley MJN, Calvi GM and Kowalsky MJ (2007). *Displacement-Based Seismic Design of Structures*. 1st Edition, ISBN: 978-8861980006, IUSS Press. https://doi.org/10.1016/S0141-0296(98)00093-5

22 Standards New Zealand (2017). "*NZS 3101.1&2:2006 Concrete Structures Standard*". Standards New Zealand, Wellington, New Zealand, 754pp. https://www.standards.govt.nz/shop/nzs-3101-1-and-22006-inc-a1-a2-a3/

23 Standards New Zealand (2007). "*NZS 3404.1&2:1997 Steel Structures Standard*". Standards New Zealand, Wellington, New Zealand, 679pp.

24 FEMA (2018). "*FEMA P-58-1, Sesimic Performance Assessment of Buildings, Volume 1 – Methodology*". Second Edition, Editors: AT Council, Federal Emergency Management Agency, Washington, D.C., USA. https://femap58.atcouncil.org/documents/fema-p-58/24-fema-p-58-volume-1-methodology-second-edition/file

25 UC Berkeley. *PEER: Pacific Earthquake Engineering Research Centre*. https://peer.berkeley.edu/

26 Porter KA (2003). "An overview of PEER's performance-based earthquake engineering methodology". *9th International Conference on Applications of Statistics and Probability in Civil Engineering (ICASP9)*, July 6-9, San Francisco.

27 Stirling M, McVerry G, Gerstenberger M, Litchfield N, Van Dissen R, Berryman K, Barnes P, Wallace L, Villamor P, Langridge R, Lamarche G, Nodder S, Reyners M, Bradley B, Rhoades D, Smith W, Nicol A, Pettinga J, Clark K and Jacobs K (2012). "National Seismic Hazard Model for New Zealand: 2010 Update". *Bulletin of the Seismological Society of America*, **102**(4): 1514-1542. https://doi.org/10.1785/0120110170

28 Bradley BA (2010). "A generalized conditional intensity measure approach and holistic ground-motion selection". *Earthquake Engineering and Structural Dynamics,* **39**(12): 1321–1342. https://doi.org/10.1002/eqe.995

29 Gerstenberger ME, Bora SS, Bradley BA, DiCaprio C, Van Dissen RJ, Atkinson GM, Chamberlain C, Christophersen A, Clark KJ and Coffey GL (2022). "*New Zealand National Seismic Hazard Model 2022 revision : Model, hazard and process overview"*. GNS Science Report, 2022/57, Lower Hutt, New Zealand, 106 pp. https://doi.org/10.21420/TB83-7X19

30 McKenna F (2011). "OpenSees: A framework for earthquake engineering simulation". *Computing in Science and Engineering*, **13**(4): 58–66. https://doi.org/10.1109/MCSE.2011.66

31 Elishakoff I (2019). *Handbook on Timoshenko-Ehrenfest Beam and Uflyand-Mindlin Plate Theories*. ISBN: 978-981-323-652-3, World Scientific Publishing Co. Pte. Ltd. Singapore, 800PP. https://doi.org/10.1142/10890

32 Otani S (1981). "Hysteretic models for reinforced concrete for earthquake analysis". *Faculty of Engineering,* **XXXVI**(2): 125-156.

33 Sarlis AAS and Constantinou MC (2010). "*Modeling triple friction pendulum isolators in program SAP2000*". University at Buffalo, Buffalo, New York, 55pp. https://doi.org/10.6084/m9.figshare.25139669.v1

34 Tsipianitis A and Tsompanakis Y (2019). "Impact of damping modeling on the seismic response of base-isolated liquid storage tanks". *Soil Dynamics and Earthquake Engineering*, **121**: 281–292. https://doi.org/10.1016/j.soildyn.2019.03.013

35 Anajafi H, Medina RA and Santini-Bell E (2019). "Effects of the improper modeling of viscous damping on the first-mode and higher-mode dominated responses of base-isolated buildings". *Earthquake Engineering and Structural Dynamics*, **49**(1): 51-73. https://doi.org/10.1002/eqe.3223

36 De Francesco G and Sullivan TJ (2022). "Formulation of localized damping models for large displacement analysis of single-degree-of-freedom inelastic systems", *Journal of Earthquake Engineering*, **26**(8): 4235-4258. https://doi.org/10.1080/13632469.2020.1826370

37 Ibarra LF, Medina RA and Krawinkler H (2005). "Hysteretic models that incorporate strength and stiffness deterioration". *Earthquake Engineering and Structural Dynamics*, **34**(12): 1489-1511. https://doi.org/10.1002/eqe.495

38 Lignos D and Krawinkler H (2011). "Deterioration modeling of steel components in support of collapse prediction of steel moment frames under earthquake loading". *Journal of Structural Engineering*, **137**(11): 1291-1302. https://doi.org/10.1061/(ASCE)ST.1943-541X.0000376

39 Lignos DG, Hartloper AR, Elkady A, Deierlein GG and Hamburger R (2019). "Proposed updates to the ASCE 41 nonlinear modeling parameters for wide-flange steel columns in support of performance-based seismic engineering". *Journal of Structural Engineering*, **145**(9): 04019083. https://doi.org/10.1061/(ASCE)ST.1943-541X.0002353

40 Krawinkler H (1978). "Shear in beam-column joints in seismic design of steel frames". *Engineering Journal*, **15**(3): 82-91.

41 Krawinkler H and Al-Ali A (1996). "Seismic demand evaluation for a 4-story steel frame structure damaged in the Northridge earthquake". *Structural Design of Tall Buildings*, **5**: 1-27. https://doi.org/10.1002/(SICI)1099-1794(199603)5:1%3C1::AID-TAL65%3E3.0.CO;2-W

42 Charney FA and Marshall J (2006). "A comparison of Krawinkler and Scissors models for including beam-column joint deformations in the analysis of moment-resisting steel frames". *Engineering Journal*, **43**(1): 31-48. https://doi.org/10.62913/engj.v43i1.868

43 Campbell TI, Kong WL and Manning DG (1990). "Laboratory investigation of the coefficient of friction in the tetrafluorethylene slide surface of a bridge bearing". *Transportation Research Record 1275*. https://onlinepubs.trb.org/Onlinepubs/trr/1990/1275/1275-007.pdf

44 Ryan KL, Okazaki T, Coria CB, Sato E and Sasaki T, "Response of hybrid isolation system during a shake table experiment of a full-scale isolated building". *Earthquake Engineering and Structural Dynamics*, **47**(11): 2214-2232. https://doi.org/10.1002/eqe.3065

45 Newmark NM (1959). "A method of computation for structural dynamics". *Journal of the Engineering Mechanics Division*, **85**(3): 67-94.

46 McGuire W, Gallagher RH and Ziemian RD (2000). *Matrix Structural Analysis*. 2nd Edition, ISBN: 9781507585139, John Wiley & Sons, New York. https://digitalcommons.bucknell.edu/books/7

47 Deierlein GG and Victorsson V (2008). "FEMA P-58/BD-3.8.3 *Fragility curves for components of steel SMF systems*". Editors: AT Council, Federal Emergency Management Agency, Washington, D.C., USA, 64pp.

48 Lignos DG, Kolios D and Miranda E (2010). "Fragility assessment of reduced beam section moment connections". *Journal of Structural Engineering*, **136**(9): 1140-1150. https://doi.org/10.1061/(ASCE)ST.1943-541X.0000214

49 Abdullah SA and Wallace JW (2019). "Drift capacity of RC structural walls with special boundary elements". *American Concrete Institute Structural Journal*, **116**(1): 183-194. https://doi.org/10.1061/(ASCE)ST.1943-541X.0003009

50 Feng D, Miyama T, Masuda K, Liu W, Zhou F, Zheng B and Li Z (2000). "A detailed experimental study on Chinese lead rubber bearing". *12th World Conference on Earthquake Engineering*, January 30 – February 2, Auckland, New Zealand, 8pp.

51 Eem S and Hahm D (2019). "Large strain nonlinear model of lead rubber bearings for beyond design basis earthquakes". *Nuclear Engineering and Technology*, **51**(2): 600-606. https://doi.org/10.1016/j.net.2018.11.001

52 Nakamura T and Kouchiyama O (2012). "Behaviors of lead rubber bearing under horizontal bi-directional loading test". *15th World Conference on Earthquake Engineering*, September 24-28, Lisbon, Portugal, 10pp.

53 Mori K, Nagashima G, Mori T, Muramatsu A and Ogata T (2022). "Dynamic characteristics tests of full-scale lead rubber bearing (LRB)". *26th International Conference on Structural Mechanics in Reactor Technology*, July 10-15, Berlin/Potsdam, Germany, 6pp.

54 Yin C, Xie L, Li A, Yang C and Wang X (2023). "Experimental and numerical investigations on the similitude effect of scaled lead rubber bearings for shaking table test". *Case Studies in Construction Materials*, **18**: e01878. https://doi.org/10.1016/j.cscm.2023.e01878

55 Muramatsu Y, Inoue K, Katoh R, Jamitani N, Sakaguchi T, Sasaki Y, Suzuki S, Sera S, Miyazaki M and Kitamura H (2004). "Test results of ultimate properties of rubber bearings for building". *Architectural Institute of Japan Journal of Technology and Design*, **10**(20): 67-70.

56 Hamaguchi H, Wake T, Yamamoto M and Kikuchi M (2019). "Practical application of lead rubber bearings with fail-safe mechanism". *Japan Architectural Review*, **2**(3): 323-339. https://doi.org/10.1002/2475-8876.12087

57 Ma SJ, Shin TM, Ryu JS, Lee JH and Koo GH (2021). "Experimental approach for the failure mode of small laminated rubber bearings for seismic isolation of nuclear components". *Applied Science*, **12**(1): 125. https://doi.org/10.3390/app12010125

58 Baker J, Bradley B and Stafford P (2021). *Seismic Hazard and Risk Analysis*. ISBN: 9781108348157, Cambridge University Press. https://doi.org/10.1017/9781108425056

59 Baker JW (2015). "Efficient analytical fragility function fitting using dynamic structural analysis". *Earthquake Spectra*, **31**(1): 579-599. https://doi.org/10.1193/021113EQS025M

60 FEMA (2018). "*FEMA P-58-3, Sesimic Performance Assessment of Buildings, Volume 3 – Supporting Electronic Materials and Background Documentations*". Third Edition, Editors: AT Council, Federal Emergency Management Agency, Washington, D.C., USA. https://femap58.atcouncil.org/supporting-materials

61 Rawlinsons Limited (2013). *Rawlinson New Zealand Construction Handbook*. 28th Edition, ISSN: 0813-5207, Rawlinsons Publications, Auckland, New Zealand, 670pp.

62 Yeow TZ, Sullivan TJ and Elwood KJ (2018). "Evaluation of fragility functions with potential relevance for use in New Zealand". *Bulletin of the New Zealand Society for Earthquake Engineering*, **51**(3): 127-144. https://doi.org/10.5459/bnzsee.51.3.127-144

63 Shegay AV (2019). "*Seismic Performance of Reinforced Concrete Walls Designed for Ductility*". PhD Dissertation, University of Auckland, Auckland, New Zealand, 415pp. https://researchspace.auckland.ac.nz/docs/uoa-docs/rights.htm

64 Fox M, Yeow T, Keen J, Sullivan T and Pavese A (2023). "New Zealand specific consequence functions for seismic loss assessment". *Bulletin of the New Zealand Society for Earthquake Engineering*, **57**(1): 18-26. https://doi.org/10.5459/bnzsee.1642

65 Retamales R, Davies R, Mosqueda G and Filiatrault A (2013). "Experimental seismic fragility of cold-formed steel framed gypsum partition walls". *Journal of Structural Engineering*, **139**(8): 1285-1293. https://doi.org/10.1061/(ASCE)ST.1943-541X.0000657

66 Jalali Y, Amiri GG and Shakouri A (2021). "Comparative response assessment of base-isolated braced-frame buildings considering effects of ductility design". *Journal of Building Engineering*, **43**: 103110. https://doi.org/10.1016/j.jobe.2021.103110